Atmos. Chem. Phys., 14, 5495–5512, 2014
www.atmos-chem-phys.net/14/5495/2014/
doi:10.5194/acp-14-5495-2014

Atmospheric Chemistry and Physics
Open Access

Eddy covariance fluxes and vertical concentration gradient measurements of NO and NO_2 over a ponderosa pine ecosystem: observational evidence for within-canopy chemical removal of NO_x

K.-E. Min[1,*], S. E. Pusede[2], E. C. Browne[2,], B. W. LaFranchi[2,***], P. J. Wooldridge[2], and R. C. Cohen[1,2]**

[1]University of California at Berkeley, Department of Earth and Planetary Science, Berkeley, USA
[2]University of California at Berkeley, Department of Chemistry, Berkeley, USA
[*]now at: NOAA Earth System Research Laboratory and Cooperative Institute for Research in Environmental Sciences, University of Colorado, Boulder, USA
[**]now at: Department of Civil & Environmental Engineering, Massachusetts Institute of Technology, Cambridge, USA
[***]now at: Lawrence Livermore National Lab, Center for Accelerator Mass Spectrometry (CAMS), Livermore, USA

Correspondence to: R. C. Cohen (rccohen@berkeley.edu)

Received: 8 April 2013 – Published in Atmos. Chem. Phys. Discuss.: 14 May 2013
Revised: 16 March 2014 – Accepted: 22 April 2014 – Published: 4 June 2014

Abstract. Exchange of NO_x ($NO+NO_2$) between the atmosphere and biosphere is important for air quality, climate change, and ecosystem nutrient dynamics. There are few direct ecosystem-scale measurements of the direction and rate of atmosphere–biosphere exchange of NO_x. As a result, a complete description of the processes affecting NO_x following emission from soils and/or plants as they transit from within the plant/forest canopy to the free atmosphere remains poorly constrained and debated. Here, we describe measurements of NO and NO_2 fluxes and vertical concentration gradients made during the Biosphere Effects on AeRosols and Photochemistry EXperiment 2009. In general, during daytime we observe upward fluxes of NO and NO_2 with countergradient fluxes of NO. We find that NO_x fluxes from the forest canopy are smaller than calculated using observed flux–gradient relationships for conserved tracers and also smaller than measured soil NO emissions. We interpret these differences as primarily due to chemistry converting NO_x to higher nitrogen oxides within the forest canopy, which might be part of a mechanistic explanation for the "canopy reduction factor" applied to soil NO_x emissions in large-scale models.

1 Introduction

The chemistry of nitrogen oxides is a major factor affecting the oxidative capacity of the atmosphere and the global burden of tropospheric ozone (Crutzen, 1973). Reactive nitrogen oxides are also a nutrient (Sparks, 2009; Takahashi et al., 2004, 2005a; Teklemariam and Sparks, 2004; Lockwood et al., 2008) and interactions between available nitrogen in ecosystems and atmospheric nitrogen are many and complex, with exchange processes altering the patterns of nitrogen availability in the biosphere (Townsend et al., 1996; Vitousek and Farrington, 1997; Vitousek et al., 1997; Holland and Lamarque, 1997; Holland et al., 1997; Ollinger et al., 2002a, b; Hietz et al., 2011). Nitrogen is the limiting nutrient for plant growth in most regions outside the tropics (Hungate et al., 2003; Galloway et al., 2004; Hietz et al., 2011), thus nitrogen deposited to the surface after atmospheric transport can act as fertilizer contributing to enhanced carbon uptake (H. Morikawa et al., 2004; T. Morikawa et al., 2004; Takahashi et al., 2004, 2005a, b; Sparks, 2009; Norby et al., 2010). For example, Norby et al. (2010) found that the availability of nitrogen was a major limiting factor for the CO_2 fertilization effect in the FACE (Free-Air CO_2 Enrichment) experiment. However, excess nitrogen deposition may impair ecosystem health (Hessen et al., 1997; Herman et al., 2001) by causing dehydration, chlorosis, or membrane damage from peroxy acetal nitrate (PAN) (Ordin et al., 1971;

Oka et al., 2004), or by inducing soil acidification and eutrophication (Makarov and Kiseleva, 1995; Pawlowski, 1997; Gbondo-Tugbawa and Driscoll, 2002; Zapletal et al., 2003; Chen et al., 2004).

A comprehensive understanding of NO_x exchange between the atmosphere and biosphere does not yet exist. Experimental studies have primarily focused on NO emissions from soils to the atmosphere (e.g., Butterbach-Bahl et al., 2002; Gasche and Papen, 2002; Gut et al., 2002a, b; Rummel et al., 2002; van Dijk et al., 2002; Dorsey et al., 2004; Duyzer et al., 2004; Feig et al., 2008; Bargsten et al., 2010; Yu et al., 2010) or on the leaf-level transfer of NO and NO_2 using branch enclosures (Hereid and Monson, 2001; Chaparro-Suarez et al., 2011; Breuninger et al., 2013; and references therein). Studies at the canopy-scale often assume a simple flux–gradient similarity relationship, meaning molecular movement is always along the gradient of high to low concentration, to infer the rate of exchange from vertically resolved observations (Mayer et al., 2011 and references therein). Direct measurements of the direction and rate of exchange (the flux) at the canopy scale are few (Wesely et al., 1982; Wildt et al., 1997; Horii, 2002, 2004; Farmer et al., 2006; Neirynck et al., 2007; Li and Wang, 2009; Brummer et al., 2013).

The base conceptual model for biosphere–atmosphere exchange of NO_x is shown in Fig. 1. In this model, NO is mainly emitted by soil microbial activity, is converted to NO_2 by reaction with O_3, and is then ultimately oxidized to nitric acid (HNO_3), which returns back to the biosphere via wet and dry deposition. The timescale of NO to NO_2 conversion by O_3 and the photolysis of NO_2 back to NO is typically ~ 100 s in the daytime, set by the photolytic and chemical reaction rates, and is comparable to the turbulent mixing time (τ_{turb}) within and out of a forest canopy. The timescale for NO_x oxidation to HNO_3 via reaction of OH with NO_2 is 3–10 h, long enough that NO_x changes by less than 1 % on the canopy residence timescale from this loss process. The rapid interconversion between NO and NO_2 implies that the individual fluxes of NO or NO_2 will not follow the form of fluxes of a conserved tracer, such as water, heat, or carbon dioxide (Vila-Guerau de Arellano et al., 1993), but the long lifetime of the sum implies the flux of NO_x, will follow that of conserved tracers.

This model of NO_x exchange is qualitatively supported by ecosystem-scale observational studies. For example, NO is observed to decrease as air is transported up through a canopy from the forest floor (e.g., Rummel et al., 2002) and the low light levels within a shaded canopy reduce NO_2 photolysis and enhance the NO_2 to NO_x ratio. For these reasons, downward NO fluxes and upward NO_2 fluxes in across the canopy top at Harvard forest have been observed as expected (e.g., Horii, 2002).

Calculations of ozone by large-scale chemical transport models parameterized with measured NO soil fluxes overpredict O_3 concentrations in comparison to aircraft and tower observations (e.g., Lerdau et al., 2000). To match observations, these models invoke a canopy reduction factor of 25–80 % (Jacob and Wofsy, 1990; Yienger and Levy, 1995; Wang and Leuning 1998). This parameter removes soil NO_x exclusively before it escapes the canopy, thus preventing its contribution to atmospheric ozone formation. Typical parameterizations use LAI (leaf area index) and SAI (stem area index) as parameters controlling the removal of soil NO_x. To our mind these mechanisms are unphysical as they do not act on all NO_x in the plant canopy – but only on soil NO_x. One motivation for our experiment is to quantify NO_x removal processes in order to develop a physically based model that treats all NO_x identically regardless of source.

At the same time, laboratory observations at the leaf scale indicate bi-directional exchanges of NO_x by plant biota, where the direction and rate of exchange is controlled by a so-called "compensation point" – a concentration above which vegetation takes up NO_2 and/or NO but below which emissions occur (Sparks et al., 2001; Raivonen et al., 2009; Chaparro-Suarez et al., 2011; Breuninger et al., 2013); however, a mechanism for the emissions remains to be discovered (Breuninger et al., 2013). Direct observations of the NO_2 compensation point are analytically challenging (Raivonen et al., 2003) and evidence suggests that compensation behavior is not fixed but rather varies by plant species, plant life cycle, and environmental conditions (Raivonen et al., 2009). That said, compensation points have been measured in the range of ambient NO_2 abundances and have been reported from 0.05 to 3 ppb (Sparks et al., 2001; Raivonen et al., 2009; Chaparro-Suarez et al., 2011; Breuninger et al., 2013). Since the NO_2 concentration in remote continental regions is typically less than 1 ppb, these observations leave open the possibility that the majority of forests on earth are a source of NO_x from direct NO_2 emissions from plants, in addition to any soil NO emissions. This is in direct contradiction with the need for canopy reduction factors that remove nitrogen oxides emitted from soils prior to its exit from plant canopies (Lerdau et al., 2000).

Recent field studies suggest the existence of rapid within-canopy chemistry affecting nitrogen oxides that is not included in the conceptual model of Fig. 1. Farmer et al. (2006) observed upward exchanges of total peroxynitrates (ΣRO_2NO_2) and HNO_3 and interpreted this as the formation of these molecules within a forest canopy. In addition, Wolfe et al. (2009) described the importance of chemical processes in speciated acyl peroxynitrate exchange, also finding observational evidence for within-canopy chemistry affecting observed fluxes. Several other experimenters have reported the occurrence of within-canopy chemistry affecting fluxes of biogenic volatile organic compounds (BVOCs) (Holzinger et al., 2005; Karl et al., 2005; Bouvier-Brown et al., 2009a, b; Park et al., 2014) and ozone (Kurpius and Goldstein, 2003). Our own recent study of peroxynitrate fluxes (Min et al., 2012) supports this idea, providing experimental evidence for upward fluxes of unidentified peroxynitrates

(F_{XPN}) formed within the forest canopy. Taken together, these studies emphasize the importance of rapid chemistry not only for determining the magnitude but also for the direction of nitrogen exchange at the biosphere–atmosphere interface.

The Biosphere Effects on AeRosols and Photochemistry EXperiment (BEARPEX) included a component designed to provide comprehensive measurements of vertical concentration gradients and fluxes of a wide suite of nitrogen oxides – NO, NO_2, total and speciated peroxynitrates, total and speciated alkyl ($\Sigma RONO_2$) and multifunctional nitrates, HNO_3, and nitrous acid (HONO) – and therefore presented a direct opportunity to test our ideas about canopy-scale NO_x exchange. Analyses of peroxynitrate (Wolfe et al., 2009; Min et al., 2012) and HONO (Ren et al., 2011) fluxes have been reported elsewhere. Here we present observations of vertical concentration gradients and fluxes of NO_2 and NO measured with laser-induced fluorescence and chemiluminescence, respectively. Fluxes are derived using the eddy covariance method. We describe relationships between gradients and fluxes, present and interpret evidence for chemical canopy reduction processes, and explore the significance of chemistry within the canopy to the import/export of NO_x from the canopy.

2 Research site and instrumentations

The data used in this work were obtained as a part of the BEARPEX 2009 experiment (15 June–31 July 2009). The experiment was conducted over a managed Ponderosa pine plantation on the western slope of the Sierra Nevada Mountain range, 75 km downwind of Sacramento, California and near the University of California Berkeley Blodgett Forest Research Station (UC-BFRS, 38°53′42.9″ N, 120°3757.9″ W; 1315 m). Many of the results from BEARPEX can be found in a special issue of Atmospheric Chemistry and Physics, http://www.atmos-chem-phys-discuss.net/special_issue89.html. A brief description of the field site and of the instrumentation relevant to this paper follows.

Analysis of the local meteorology by Choi et al. (2011) and Dillon et al. (2002) indicate that in the summer (May–September), winds at the BEARPEX site are characterized by daytime southwesterlies (210–240°) and nighttime northeasterlies (30°) with little variability. The major source of anthropogenic emissions in the region is the city of Sacramento and its suburbs. There is a line source of oak trees that are strong isoprene emitters aligned perpendicular to the flow between the urban center and the site. This source distribution, in combination with the regular winds, results in low concentrations of trace gases with anthropogenic or isoprene sources early in the morning and higher concentrations in air transported from the west later in day (Dillon et al. 2002; Day et al., 2003; Murphy et al., 2007; Choi et al., 2011; LaFranchi et al., 2011). The two sources arrive at distinct times; with air influenced primarily by isoprene arriving at approximately noon and the urban plume combined with the isoprene source arriving about 3–4 h later.

There were two sampling towers at the site: a 15 m walk-up tower on the south side of the site (hereafter south tower) and an 18 m scaffolding tower located 10 m north of the south tower (hereafter north tower). On the south tower, temperature, relative humidity, wind speed, net radiation, photosynthetically active radiation (PAR), water vapor, carbon dioxide (CO_2), and O_3 were monitored at 5 heights (1.2, 3.0, 4.9, 8.75, and 12.5 m above the forest floor). At 12.5 m, fluxes of water vapor, CO_2, and O_3 were measured. Vertical gradients of temperature, relative humidity, and wind speed were also measured on the north tower at 5 heights (1.2, 5.4, 9.2, 13.3, and 17.5 m above the forest floor). Measurements from the north tower or on an adjacent height-adjustable lift included NO, NO_2, HONO, total peroxy nitrates (ΣPNs, RO_2NO_2), total alkyl and multifunctional nitrates (ΣAN, $RONO_2$), HNO_3, hydroxyl radical (OH), hydroxy peroxy radical (HO_2), OH reactivity, O_3, several individual PNs, several individual ANs, numerous volatile organic compounds (VOCs) including many biogenic VOCs (BVOCs), formaldehyde (HCHO), glyoxal, methylglyoxal, organic peroxides, and aerosol chemical and physical properties. Needle temperature, soil moisture, soil temperature, and soil heat flux were also monitored. All measurements were made at the 17.5 m level and many were additionally recorded at one or more of the following heights: 0.5, 1.2, 5.4, 9.2, and 13.3 m. For simplicity, we refer to these measurement heights as 0.5, 1, 5, 9, 13 and 18 m. In addition, soil NO measurements were made using dynamic chambers on 2 July (09:15, 13:40 and 18:10), 12 (08:25 and 16:20) and 30 (08:50 and 16:10) to provide an observational constraint on the soil NO emission at this site: soil NO flux from four different locations (15 min sampling each) were measured to represent morning, midday and the late afternoon time window.

The upper canopy at this site was mainly *Pinus ponderosa* L., with a few scattered Douglas fir, white fir, and incense cedar. The understory was primarily mountain whitethorn (*Ceanothus cordulatus*) and manzanita (*Arctostaphylos* species) shrubs (see Misson et al., 2005, for a more detailed site description and history). The mean tree height was 8.8 m and the leaf area index (LAI) was $3.7\,m^2\,m^{-2}$, based on a tree survey conducted on 17 July 2009.

NO was measured using a custom-built two-channel chemiluminescence NO detection system (2ch-CL) and NO_2 with two separate thermal-dissociation laser-induced fluorescence (TD-LIF) systems. The sampling inlets for NO and NO_2 were collocated at 0.5, 5, 9 and 18 m on the north tower and represent the forest floor, mid-canopy, top canopy, and above canopy, respectively. At 18 m, fluxes of NO and NO_2 were monitored along with 3-D wind and temperature

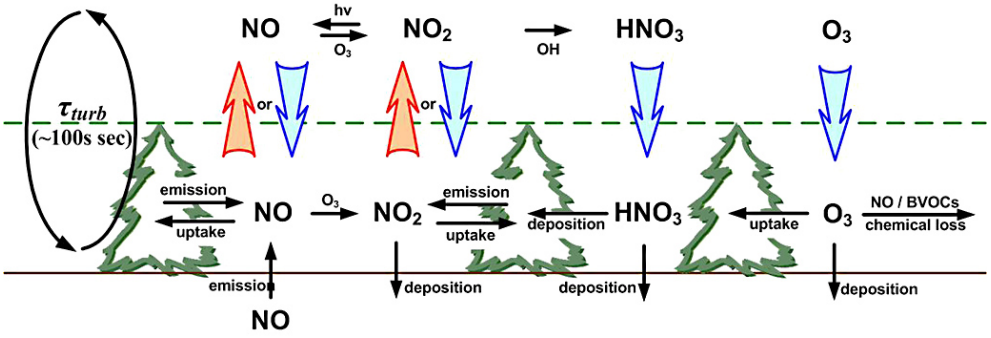

Figure 1. Schematic of the various interactions involved in the exchange of nitrogen oxides between the atmosphere and the forest canopy. Bold arrows in blue (downward) and red (upward) represent the direction of the flux of each species across the canopy surface.

from a sonic anemometer (Campbell Scientific CSAT3 3-D Sonic Anemometer). The measurements were combined to infer fluxes using an eddy covariance method (EC) (see Sect. 3). The sonic anemometer was pointing into the mean daytime wind stream with 0.02 m vertical displacement and 0.2 m horizontal displacement from the NO and NO_2 inlets.

The 2ch-CL system for the NO flux and vertical gradient measurements was based on the standard O_3 chemiluminescence method. A detailed description of the operating principle can be found elsewhere (Drummond et al., 1985 and references therein). Briefly, ambient NO is combined with an excess of O_3 generated by electric discharge in O_2. The reaction of NO and O_3 produces excited-state NO_2 molecules, which then fluoresce. Two gold-plated detection cells were used for simultaneous flux and vertically resolved concentration measurements. The signals from photocathodes (flux channel: EMI 9658B, gradient channel: Hamamatsu H7421-50) were acquired at 5 Hz. The cell pressures were maintained at 8–8.7 Torr with pressure restricted at the inlet and a fluorinated oil-sealed rotary vane pump. During the sampling mode, 100 % of the ozone flow was added directly into the detection cell to monitor the ambient NO concentration (for 24 s). The background signal was monitored by adding 50 % of the O_3 to the sampling air prior to the detection cell to titrate ~ 90 % NO (for 6 s). Incomplete titration of NO was employed to limit interferences from fluorescence of vibrationally excited OH molecules produced in the reaction of ozone with alkenes (Drummond et al., 1985). The other 50 % of the ozone was added directly to the cell to minimize flow changes within the reaction cell between the sampling and the background mode. Our own laboratory experiments confirm that a wide variety of terpenes react with ozone to efficiently produce vibrationally excited OH and we configured the instrument to minimize detection of this signal.

Two TD-LIF systems were used for simultaneous flux and vertical gradient measurements of NO_2 and the higher nitrogen oxide species ΣPNs, ΣANs and HNO_3. Details of LIF detection of NO_2 (Thornton et al., 2000), thermal dissociation of higher nitrogen oxides (Day et al., 2002), and application to EC flux measurement (Farmer et al., 2006) are described elsewhere. Briefly, thermal dissociation of each class of higher oxide generates NO_2 and a companion radical at the characteristic temperatures ~ 180 °C for ΣPNs, ~ 350 °C for ΣANs, and ~ 600 °C for HNO_3, (Day et al., 2002). The thermal dissociation is followed by detection of NO_2 by LIF. In both TD-LIF systems, excitation at 585 nm was provided by frequency doubled Nd:YAG (Spectra Physics, average power of 2 W at 532 nm, 30 ns pulse length) pumping a custom-built tunable dye laser operating at 8 kHz. The wavelength of the dye laser beam was tuned to a specific, narrow rovibronic feature of NO2 by rotating an etalon within the dye cavity. We alternated the laser frequency between a strong NO_2 resonance (8 s) and the weak continuum adsorption (4 s) to maintain a frequency lock on the spectral feature of interest. By adapting a supersonic expansion technique, we acquired ~ 10-fold higher sensitivity to NO_2 (Cleary et al., 2002). The fluorescence signal 700 nm long was collected and imaged onto a red sensitive photocathode (Hamamatsu H7421-50). Gated photon counting techniques (Stanford Research Systems, SRS 400) were employed to discriminate against prompt background signals. Laboratory measurements and comparison in the field showed the two TD-LIF instruments to have calibrations that were identical to within 4 % (slope: 1.0 ± 0.10, R^2: 0.92). Allowing the intercept to vary from zero did not change the slope or R^2.

Cell pressures in the flux system were reduced to 0.17–0.19 Torr to achieve the high expansion ratios for the supersonic jet cooling by using Lysholm twin screw blowers (Whipple model 2300 superchargers) backed by an oil-sealed rotary vane pump. The jet nozzles and this pump system combined to maintain a 580–700 sccm flow through each of the four cells (total flow of 2300 sccm). To reduce high frequency damping of turbulent eddies and interference from secondary chemistry in the heated section of the inlet and sampling lines (30 m), we added a diaphragm bypass pump and maintained the total flow of a 13 000 sccm. For the gradient system, critical orifices as pressures restrictors (AirLogic, F-2815-251-B85, 0.025" orifice diameter) were placed at the

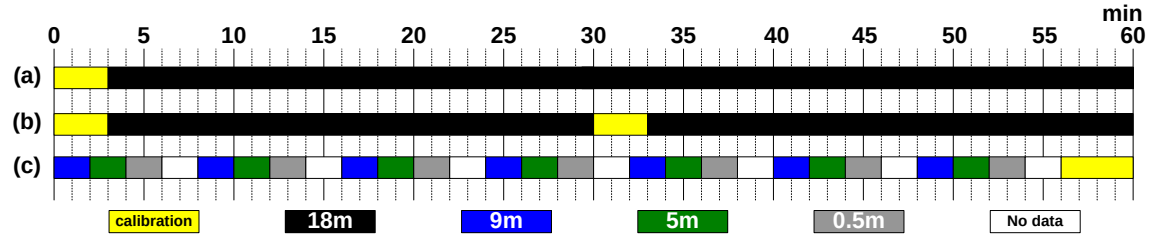

Figure 2. Data collection scheme for fluxes of NO (**a**: 2ch-CL) and NO_2 (**b**: TD-LIF) and vertical gradient **(c)** measurements. Colors represent the different measurement heights: 18 m (black), 9 m (blue), 5 m (green), and 0.5 m (gray). Yellow periods are calibration cycles and white periods represent times when diagnostics were collected.

end of the inlet manifold to reduce the pressure along the sampling line.

Calibrations in the field were repeated once (gradient measurement of NO and NO_2 and flux measurement of NO) or twice (flux measurement of NO_2) per hour. NO_2 standard gas (4.9 ± 0.2 ppm No_x in N_2, PRAXAIR) was diluted to 3–20 ppb in zero air and added to system at the inlet tip. For NO, 2.25–6.7 ppb of NO (5.4 ppm ± 5 % NO in N_2, PRAXAIR) was diluted with zero air and added at the inlet. Both cylinders were referenced to a library of calibration standards maintained in our laboratory. The mixing ratios were corrected (< 2 %) for quenching by water using north tower RH measurements. To evaluate the background counts due to cell scatter and photocathode dark noise, we flowed excess zero air into the inlet once/twice per hour. The diagnostics for the NO and NO_2 flux instruments (calibration and zeroing) were completed within the first 3 min of every 30 min (Fig. 2a). Flux data for both species were collected at 18 m during the first 27 min, from the 3 to the 30 min, and for the last 27 min, from the 33 to the 60 min each hour (Fig. 2a). NO and NO_2 at the lower levels were measured by switching between the 9, 5, and 0.5 m heights and sampling at each height for 2 min (Fig. 2b); the first 5 s for data of each level after the valve switching from another height were deleted to insure the measurement corresponded to the height in question. Calibrations and zeros were completed in the last 4 min from 56 to 60 min of every hour for both gradient systems (Fig. 2b).

Data affected by exhaust plumes from a nearby propane electrical generator (mostly at night) and the infrequent wafts of car exhaust were removed prior to analysis. These spikes were defined as variations in the NO or NO_2 concentration in excess of 3 times the standard deviation of the 10 min running mean. A few remaining spikes were identified through correlations with CO and removed by hand. Over the campaign, the NO_2 detection limit (defined as $S/N = 2$) was ∼ 45 ppt for 1 s corresponding to 1.3 ppt for a 30 min average for the flux system, and was ∼ 10 ppt 1 min (4.0 ppt for 30 min) for the gradient system. The NO detection limit for flux cell was ∼ 58 ppt for 1 s (1.6 ppt for 30 min averages) and for the gradient cell, ∼ 29 ppt for 1 min (11.5 ppt for 30 min averages) at midday (12:00–14:00, local time).

3 Eddy covariance calculation

The flux (F_c) of an atmospheric constituent (c) (i.e., the turbulent mass transport of c through a vertical reference layer) can be evaluated from the covariance between the concentration of c and the vertical wind (w) in a method known as eddy covariance (EC) and is represented mathematically by Eq. (1) (e.g., Foken, 2006; Lee et al., 2004; McMillen, 1988).

$$F_c = \int_{t0}^{t} w'c' \mathrm{d}t = \frac{1}{n}\sum_{i=1}^{n}(w_i - \overline{w})(c_i - \overline{c}) = \overline{w'c'} \quad (1)$$

In Eq. (1), primes represent the deviation from the mean, subscripts i refer to individual high-time resolution measurements (NO or NO_2), and bars indicates the mean over the averaging interval. In this work, the flux of NO_x, F_{NO_x}, is defined as the sum of the separately calculated F_{NO} and F_{NO_2}. We checked this calculation by comparing with F_{NO_x}, calculated by first adding the NO and NO_2 concentrations and found the two methods agree to within 18 %, which is smaller then propagated errors of F_{NO_x} estimated (Table 1) from the sum of F_{NO} and F_{NO_2}.

We used 5 Hz data for the flux calculations and averaged for ∼ 30 min, a timescale that spanned the range of the major flux-carrying eddies at this site (e.g., Wolfe et al., 2009; Farmer et al., 2006). Prior to calculating fluxes, we rotated the wind measurements to ensure that the vertical winds were normal to the shear plane (Baldocchi et al., 1988; McMillen, 1988). We also de-spiked and de-trended the concentration data, where spikes were defined as data greater than 3 times the standard deviation of the 10 min running mean, and where the 10 min running mean was also used for de-trending.

To synchronize the timing of wind and concentration measurements, the lag was determined from the maximum in covariance of the deviation from the mean of vertical wind speed and concentration; the cross-correlation between scalar and vertical wind were calculated for every 30 min and then averaged with multiple time windows (i.e., morning: 10:00–12:00, midday: 12:00–14:00, afternoon: 14:00–16:00) to determine the precise lag time. We did not find any

Table 1. Estimated flux analysis errors.

	Source of error	F_{NO}	F_{NO_2}	F_{NO_x}
Systematic error	Data acquisition scheme	< 2 % (unbiased)	< 3 % (unbiased)	< 4 % (unbiased)
	Sensor separation and High frequency damping	<2 % (underestimated)	<2 % (underestimated)	<3 % (underestimated)
	Instrumental response time	< 0.2 % (underestimated)	< 0.7 % (underestimated)	< 0.7 % (underestimated)
	Absolute concentration estimation	< 7 % (unbiased)	< 5 % (unbiased)	< 9 % (unbiased)
	Total	< 8 %	< 6 %	< 10 %
Random error	Instrument noise[a]	< 20 % (unbiased)	< 10 % (unbiased)	< 23 % (unbiased)
	Detection limit concept[b]	< 25 % (unbiased)	< 21 % (unbiased)	< 33 % (unbiased)

[a] Errors over half an hour. [b] Estimated form the ratio of covariances at true lag and several lag times far from the true lag (±230–250 s).

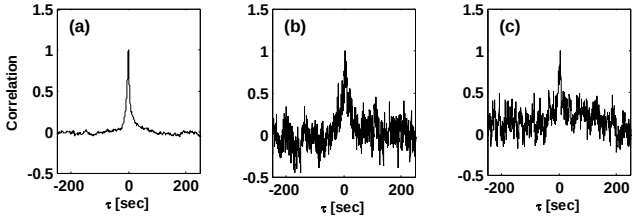

Figure 3. Lag calculation of **(a)** $w'T'$, **(b)** $w'NO'$ and **(c)** $w'NO_2'$. Highest normalized correlation between wind and temperature, NO or NO_2 were observed as expected; 0 s for wind and temperature, 1.4 and 2.6 s for NO and NO_2.

change in lag time with time of day. We compared the lag times in the different periods of the experiment and found no drift over the duration of the experiment. Three periods were tested, 18–30 June, 1 –15 July and 16–30 July, and each calculated lag time agreed within 1 data point (0.2 s) for both NO and NO_2. Figure 3a–c show the lag correlation between wind and temperature, NO, and NO_2, respectively. The data plotted in Fig. 3 are the averaged midday (12:00–14:00) lag over the whole field campaign and are representative of lag correlation plots throughout the experiment. As expected, zero lag was observed between vertical wind speed and temperature as both quantities are synchronously measured by the same instrument, the sonic anemometer. Lag times for NO and NO_2 were measured to be 1.4 and 2.6 s, times that were consistent with transport times in the tubing (< 0.8 s) plus the time difference between sonic anemometer computer and computers for 2ch-CL and TD-LIF.

To assure that each 30 min flux was representative of the average surface exchange over the sampling period, we tested the calculated fluxes for stationarity (Farmer et al., 2006; Foken 2006; Wolfe et al., 2009). To do this, five equally divided subsets of each 30 min flux period, F_{sub}, were averaged and compared with that of the full period, $F_{30\,min}$. If F_{sub} differed from $F_{30\,min}$ by more than 30 % then that measurement period was defined as non-stationary and that half-hour excluded from further analysis (Foken and Wichura, 1996). Also, the calculated flux data with a tilt angle greater than 5° from the wind rotation (Lee et al., 2004) and with a friction velocity smaller than 0.1 m s^{-1} or larger than 1.5 m s^{-1} (Foken 2006) were excluded for further analysis. We tested this using friction velocity in the range 0.05–0.2 m s^{-1} as filtering criteria. Changes in this range do not affect our conclusion, which is consistent with previously reported analyses of fluxes at this site (Farmer et al., 2006).

Approximately 2/3 of the daytime and half of the nighttime data remained after application of these filters. We estimate the total uncertainty in F_{NO_x} by combining the systematic and random error terms in F_{NO} and F_{NO_2} flux estimations following Moore et al. (1986) and Massman (1991). Each of the individual elements is summarized in Table 1 and detailed procedures are described in Farmer et al. (2006) and Wolfe et al. (2009).

The total systematic uncertainties for F_{NO} and F_{NO_2} (< 8 and < 6 %, respectively) are calculated from the root mean square of errors from instrument calibration (7 and 5 % for NO and NO_2, respectively; see Day et al., 2002), sensor separation and inlet dampening (< 2 % for both F_{NO} and F_{NO_2}), instrument time response (< 0.2 % and < 0.7 % for daytime F_{NO} and F_{NO_2}, respectively) and data acquisition sequencing (i.e., laser line-locking cycling for TD-LIF system: < 3 % or frequent background checking for 2ch-CL system: < 2 %, estimated from the sensible heat flux calculation

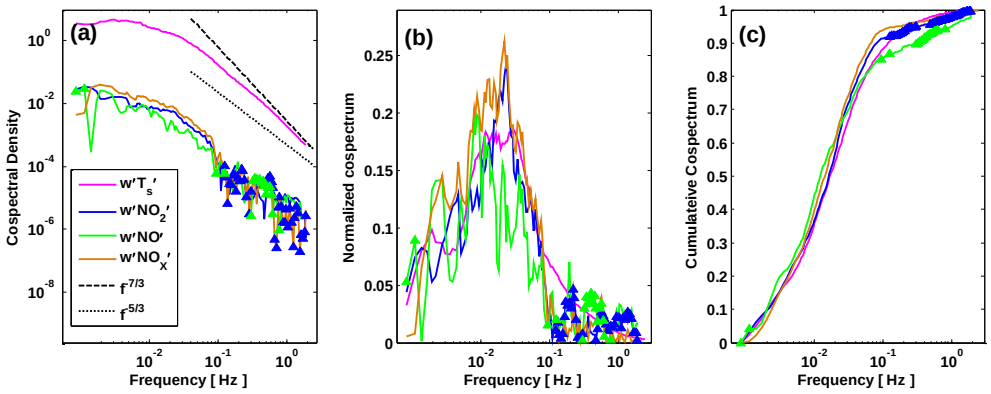

Figure 4. Equally spaced logarithmic averaged (150 bins) absolute cospectral density **(a)**, frequency weighted cospectrum **(b)**, and normalized cumulative distributions of the cospectra of temperature (magenta) NO (green), NO_2 (blue) and NO_x (yellow) **(c)** with vertical wind from 11:00–12:00 through out the whole field campaign when the chemical perturbation is small. Closed triangles represent the absolute value of the negative cospectral density, which has the opposite sign to the general flux direction. The black dotted lines in **(a)** are lines with slopes of $-7/3$ and $-5/3$ (see related text).

using temperature data coincident with the NO or NO_2 data. The gaps in the data acquisition sequence are replaced by the mean concentration for 27 min.)

Two different methods were used to estimate the precision (random errors) of the flux measurements: (1) estimates based on the finite precision of photon counting and (2) the variance of the flux calculation with lag determination. The precision estimates based on photon-counting statistics follow Farmer et al. (2006) and are 0.08 ppt m s^{-1} (20 %) and 0.14 ppt m s^{-1} (10 %) for F_{NO} and F_{NO_2}, respectively, over half an hour. This estimate is similar to but slightly smaller than the precision of 25 % (0.10 ppt m s^{-1} for F_{NO}) and 21 % (0.29 ppt m s^{-1} for F_{NO_2}) estimated from the flux variance over a range of lag times far from the true lag (Ruuskanen et al., 2011), indicating the presence of other sources of random error in the measurement in addition to photon counting. One common measure of the flux detection limit is 2 times the standard deviation of the covariance within the time window far from the peak covariance. We use $\pm 230 \sim 250$ s during the daytime (09:00–18:00) (Table 1). The value is not significantly different if we use smaller time windows. For cases such as ours, where fluxes are bi-directional, an alternative approach to estimating a detection limit based on the absolute cross-correlation has been proposed by Park et al. (2013). By either metric the fluxes we report are well above the noise.

Spectral analyses of the fluxes are shown in Fig. 4 and include the cospectral density (Fig. 4a), the normalized cospectrum (Fig. 4b), and the absolute value of the normalized cumulative cospectrum (Fig. 4c) for temperature, NO, NO_2 and NO_x. We show each measurement averaged for the time interval 11:00–12:00 throughout the whole field campaign. By analyzing the NO_x (yellow) cospectrum, rather than the spectra of NO (green) and NO_2 (blue) separately, we are insensitive to the effects of the rapid chemical conversion between NO and NO_2. The absolute values of the negative cospectral density were plotted as closed triangles in Fig. 4. The figures show that we capture the full range of eddies that contribute to the flux.

The spectral analysis of NO_x provides additional evidence that our instruments for NO and NO_2 observe the full range of flux-carrying eddies at this site. We see in Figure 4a that the observed cospectral density of sensible heat, $w'T'$, decreases in the inertial sub-range (above 0.003 Hz) with a linear slope between that predicted by surface layer theory ($-5/3$) (Kaimal and Finnigan, 1994) and the slope for sensible heat observed previously at this site ($-7/3$) (Farmer et al., 2006; Wolfe et al., 2009). Because the cospectral density of the vertical wind speed and NO, NO_2 and NO_x are parallel to that of sensible heat, we have confidence that our sampling interval and data acquisition time resolution were sufficient to capture the flux-carrying eddies. Additionally, the comparable behavior observed in the $w'T'$, $w'NO'$, $w'NO_2'$, and $w'NO_x'$ cospectrum confirm that those frequencies characteristic of our instruments' sampling and operative cycles (e.g., regular patterns in on/off sampling sequencing in both NO and NO_2) do not interfere with the measurements of fluxes. The parallel slopes of $w'T'$, $w'NO'$, $w'NO_2'$, and $w'NO_x'$ in the inertial sub-range (above 0.003 Hz), demonstrates that measured fluxes were not significantly dampened by the transport along the sampling lines. Finally, we note that we observe both positive and negative cospectral density for NO, NO_2 and NO_x fluxes at different frequencies. In Fig. 4a–c triangles refer to negative and solid lines to positive cospectral density. Few studies report sign changes in a scalar cospectrum other than that of momentum flux (Wolfe et al., 2009; DiGangi et al., 2011; Park et al., 2014). Details of the cospectral analysis along with sign changes and the discussion of their underlying physical mechanisms will be presented elsewhere (Min et al., 2014). Briefly, we find that chemical reactions forming higher oxides of nitrogen from

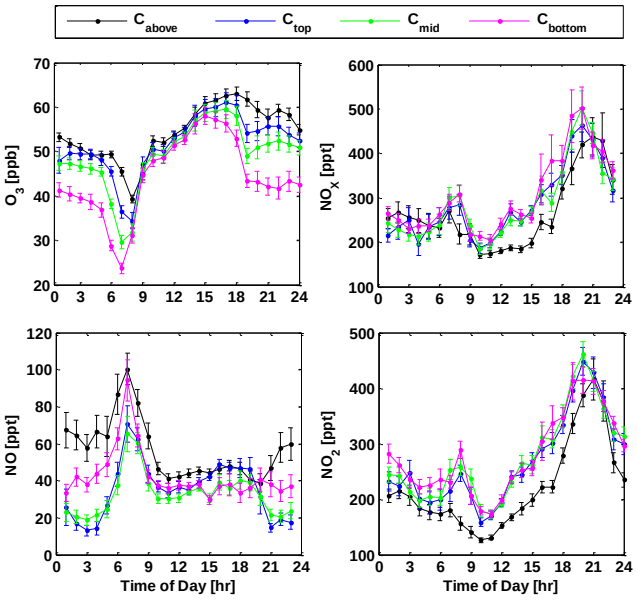

Figure 5. Diurnal patterns of O_3 (south tower), NO_x, NO, and NO_2. The data are 1-hour mean values and the error bars represent the variation defined as the observed variability ($\pm 1\sigma$) divided by square root of the number of measurements in that time bin. Colors represent the measurement heights: above canopy (18 m) in black, top canopy (9 m) in blue, middle canopy (5 m) in green, and forest floor (1.5 m for O_3 and 0.5 m for NO and NO_2) in magenta.

NO_x are one possible cause of frequent sign change only in the scalar cospectrum.

The normalized cospectrum, shown in Fig. 4b, indicates the fraction of the total flux at each frequency. It is calculated as the cospectra multiplied by the frequency and divided by the covariance of temperature, NO, NO_2 or NO_x, with the vertical wind, which is the integrated value under the curve. Generally, the shape of the normalized cospectrum of $w'\mathrm{NO}'$, $w'\mathrm{NO}'_2$, and $w'\mathrm{NO}'_x$ are similar to that of $w'T'$ with a maximum in the range 0.005–0.1 Hz (200–210 s), values consistent with previous observations at this site (Farmer et al., 2006; Wolfe et al., 2009; Park et al., 2014). A steeper falloff at high frequencies (> 0.01 Hz) for $w'\mathrm{NO}'_x$ and $w'\mathrm{NO}'_2$ (especially in the afternoon, not shown) than for $w'T'$ was reported in previous studies of PAN at this site (Wolfe et al., 2009), in a Loblolly pine forest (Turnipseed et al., 2006), and for HCHO in a ponderosa pine forest in Colorado (DiGangi et al., 2011) as well as for a variety of BVOCs at this site (Park et al., 2014). The peaks and valleys in $w'\mathrm{NO}'_2$ seen at frequencies of 0.002, 0.005 and 0.015–0.03 Hz are associated with valleys and peaks of $w'\mathrm{NO}'$, which may be an indication of chemical conversion between NO and NO_2 during transport.

Figure 4c shows the absolute value of the normalized cumulative distributions of the cospectra of $w'T'$, $w'\mathrm{NO}'$, $w'\mathrm{NO}'_2$, and $w'\mathrm{NO}'_x$. The cumulative distribution for $w'T'$ approaches a horizontal asymptote at both ends of the spectrum, providing additional confirmation that the sampling interval and time resolution was both long enough and fast enough to capture all the important flux-carrying eddies. The patterns of $w'\mathrm{NO}'_x$ as well as $w'\mathrm{NO}'$, $w'\mathrm{NO}'_2$ are generally comparable to that of $w'T'$, except for frequencies in the ranges 0.1–1 Hz, where cospectra signs are changing. Here, we use the the absolute magnitude frequency weighted normalized cospectra of $w'\mathrm{NO}'$, $w'\mathrm{NO}'_2$, and $w'\mathrm{NO}'_x$ for the cumulation noting that the frequencies of $w'\mathrm{NO}'$, $w'\mathrm{NO}'_2$, and $w'\mathrm{NO}'_x$ that have a negative cospectrum vary with time of day, suggesting they are not internally generated, but are rather the result of time-of-day-dependent atmospheric processes. Detailed discussion of these features will be presented elsewhere (Min et al., 2014).

4 Gradients and fluxes

The diurnal variations in the concentrations of O_3, NO_x, NO, and NO_2 averaged over the whole field campaign, except the short time periods during rain events on 2 and 11 July, are shown in Fig. 5 and are similar to previous observations at this site (Day et al., 2003; Farmer et al., 2006). There is no significant difference between mean and median values, indicating the data has little skew. The patterns are affected by transport from the city of Sacramento, local emission, deposition, and chemistry. O_3, NO_x, and NO_2 increase as air is transported in from the west, carrying the remnants of emissions from Sacramento, and reach a maximum after sunset between 18:00 and 21:00. Generally, NO can be thought of as controlled by the amount of soil NO_x and local photochemistry. In the morning, we observe an enhancement in NO and NO_2 and a decrease in O_3. We observe the highest NO concentrations above the canopy, decreasing NO within the forest, and increasing NO concentrations again near the forest floor – except in the late afternoon when turbulent mixing is strongest and dry soils result in NO emissions that are at their daily minimum. This pattern is consistent with our soil flux measurements, showing the lowest signal in late afternoon. At night there is some local contamination from the propane generator at the site.

Typical NO mixing ratios above the canopy during BEARPEX 2009 ranged from 10 to 100 ppt with a daytime (09:00–18:00) mean (median) $\pm 1\sigma$ of 45 (39) $\pm$ 19 ppt. This concentration is $\sim$ 20 % lower than observed at this site during the same time of year in 2001 (Day et al., 2003). The highest NO concentration near the forest floor was 270 ppt, following rainfall on the evening of 11 July. The mixing ratio of NO_2 above the canopy varied from 80 to 550 ppt, with a daytime mean concentration of 188 (176) $\pm$ 86 ppt. This is a 65 % decrease from the 533 ppt mean observed in 2001 (Day et al., 2003) and is in agreement with previously reported NO_x decreases in upwind Sacramento of approximately 13 % yr^{-1}, which accumulates to an approximately

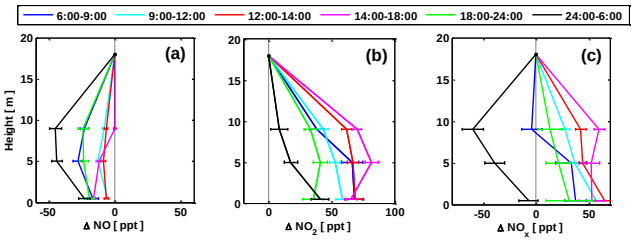

Figure 6. Vertical gradients of NO, NO_2, and NO_x. Dot and whiskers represent means and standard errors of the mixing ratio enhancement at each height. The colors represent the enhancement at six different times of day through the complete diurnal cycle: early morning (06:00–09:00, blue), late morning (09:00–12:00, cyan), midday (12:00–14:00, orange), afternoon (14:00–18:00, magenta), evening (18:00–24:00, green) and night (24:00–06:00, black).

67 % decrease between 2001 and 2009 (Russell et al., 2010; LaFranchi et al., 2011).

Figure 6 shows the vertical gradients of NO, NO_2, and NO_x throughout the course of the day over the entire field campaign: early morning (06:00–09:00, blue), late morning (09:00–12:00, cyan), midday (12:00–14:00, red), afternoon (14:00–18:00, magenta), evening (18:00–24:00, green) and night (24:00–06:00, black). A few examples of daily profiles can be found from the Supplement Sect. S1. Of these, only the pair of NO_2 measurement at 0.5 and 5m are not significantly different ($p = 0.7$) which we interprete to confirm that the gradient we observedis not a bias from the measurement methods.

For the purpose of discussion we define an enhancement factor (ΔX) to be the concentration difference between each height and that measured above the canopy ($\Delta X = X_i - X_{18m}$). Positive values of ΔX indicate concentration enhancements, and negative values indicate depleted concentrations relative to the above-canopy value. As shown in Fig. 6, NO was depleted within the canopy (a) and NO_2 was enhanced at all times of day (b). In general, we observed the least NO depletion near the soil (except at night) and the largest NO_2 enhancement at the mid- and top-canopy heights. This pattern is qualitatively explained by emissions of NO at the soil, followed by the conversion of NO to NO_2 until the steady-state ratio is established by the reaction of NO with O_3 and photolysis of NO_2.

If soil NO emissions and the chemical cycling of NO/NO_2 were the only two process controlling NO_x, then we would expect the gradient in the sum of NO and NO_2 to be a straight line connecting the enhanced concentration at forest floor with the above-canopy (boundary layer) value so long as sufficiently strong turbulent mixing exists (Vila-Guerau de Arellano et al., 1993; Gao et al., 1991; Jacob and Wofsy, 1990). This, however, is not what we observe (Fig. 6c). Rather we observe a NO_x enhancement within the canopy during the day and depletion at night. In addition, the enhancement at the forest-floor, mid-canopy, and top-canopy heights changes within different time windows, indicating the existence of processes other than soil NO emission and interconversion of NO and NO_2. For example, the within-canopy gradients at 06:00–09:00 (blue) and 14:00–18:00 (magenta) are opposite each other; the 06:00–09:00 NO_x gradient indicates the existence of a NO_x sink process as the height increases from mid- to top-canopy, while the 14:00–18:00 gradient indicates a NO_x source. While there have been a number of indirect lines of evidence for the idea that processes other than soil NO emission and NO/NO_2 photochemical partitioning affect NO_x fluxes (Jacob and Wofsy 1990; Yienger and Levy 1995; Wang and Leuning 1998; Lerdau et al., 2000; Wolfe et al., 2011; Min et al., 2012; Seok et al., 2013), to our knowledge these observations provide the first direct observational evidence.

In Fig. 7a–c, we show the eddy covariance fluxes of NO, NO_2 and NO_x as well as sensible heat. In this figure and for the remainder of the analysis, we include data only when F_{NO}, F_{NO_2} and F_{sht} (flux of sensible heat) are all available. We observed upward fluxes from 09:00 to 15:00. Fluxes of NO and NO_x were slightly downward from 06:00–09:00. The midday (12:00–14:00) median fluxes of NO, NO_2 and NO_x are 0.32 ± 0.27, 0.67 ± 0.21 and 1.0 ± 0.43 ppt m s^{-1}. A comparison of the direction of the observed flux of NO_2 and NO_x to the gradients in Figures 6b and c gives a picture of molecule movement consistent with standard ideas of turbulent transport moving material from a region of high to low concentration. For NO, the direction of the flux is counter to that of the concentration gradient.

The observed midday fluxes of NO_x of 1.0 ± 0.43 ppt m s^{-1} are similar to midday soil NO emission measured at this site in the late afternoon of 0.05–0.8 ppt m s^{-1}. Larger fluxes were observed in the morning, 2.6–5.2 ppt m s^{-1}, and much larger fluxes were measured after rain, 21.6 ppt m s^{-1}. These soil NO_x fluxes are at the low end of measurements in the region – which were all made much closer to urban centers where N deposition to the soils is much larger. Our own chamber measurements were in a nearby clearing and may have been in soil that was drier, and hence with lower soil NO_x emission than is representative of the fetch at the site. At the Schubert Watershed at the Sierra Nevada Foothill Research and Extension Center in an oak forest, soil NO_x emissions of 5.8–15 ppt m s^{-1} were observed during the summer (Herman et al., 2003) and typical soil NO fluxes reported for other locations in California are 2–20 ppt m s^{-1} (Anderson and Poth, 1989; Davidson et al., 1993).

To evaluate the contribution of soil NO emission to the NO_2 flux by the reaction with O_3, we divide our system into a soil NO emission layer and a chemical conversion layer, where the latter layer includes the within- and above-canopy measurement heights. The noontime (12:00–14:00) ratio of NO and NO_2 in the conversion layer (estimated as the averaged value over all measured heights) is 1 : 4.7. Thus, after reaching steady state with ozone, we expect 0.82 NO_2

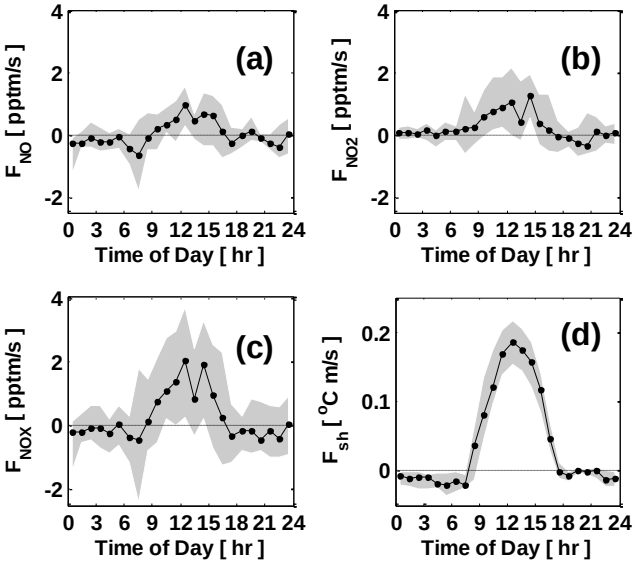

Figure 7. Diurnal patterns of the NO, NO_2, NO_x, and sensible heat fluxes in panels **(a)**, **(b)**, **(c)**, and **(d)**, respectively. All fluxes are upward, indicating molecular motion from forest to atmosphere. Median midday (12:00–14:00) fluxes are 0.32 ± 0.27, 0.67 ± 0.21, and 1.0 ± 0.43 ppt m s^{-1} for NO, NO_2, and NO_x and that of sensible heat flux is 0.21 ± 0.08 °C m s^{-1}. Black lines represent means and the gray areas give 25–75 % of flux data for hourly bins.

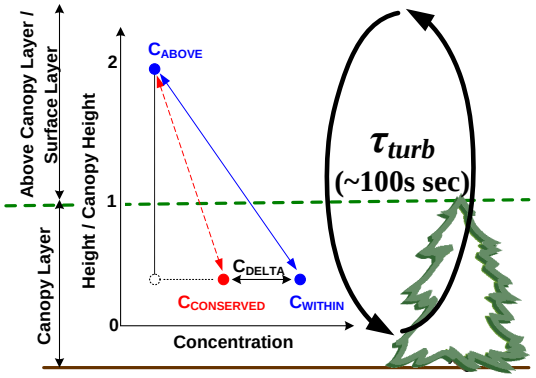

Figure 8. Schematic of our two-layered model based on the localized near field, LNF, concept. C_{ABOVE} represents the reference concentration, which for the above-canopy layer is defined as the measured concentration at a height of 18 m. C_{WITHIN} is the measured concentration within the canopy, defined as the averaged concentration at 0.5, 5, and 9 m. $C_{CONSERVED}$ is the estimated concentration based on the measured eddy covariance flux and the eddy diffusivity calculated from sensible heat flux. C_{DELTA} is the difference between C_{WITHIN} and $C_{CONSERVED}$ and is a measure of the importance of non-conservative processes.

molecules for every NO molecule emitted from the soil emission layer. This is a lower limit, at other times of day there can be as much as 1 NO_2 per NO. The NO emitted has a negligible effect on the O_3 flux consistent with previous analyses of ozone flux (Kurpius and Goldstein, 2003). Additional details about O_3 flux measurements at this site can be found elsewhere (Fares et al., 2010).

Using the lowest measured soil NO emission rate measured in the morning as well as the observed O_3 at this site, we calculate the conversion of NO to NO_2 induces a 2.38 ppt m s^{-1} NO_2 flux, a number which is 3.5 times larger than the observed NO_2 flux (0.67 ± 0.21 ppt m s^{-1}), another piece of evidence supporting the existence of a canopy reduction process for NO_2.

5 Analysis

For a conserved tracer, the direction and magnitude of the flux is controlled by the local concentration gradient and the rate of vertical mixing – the tracer moving from high to low abundance and the rate of movement determined by the strength of both the gradient and the turbulent mixing. This concept is known as flux–gradient similarity or Bowen ratio theory, and is often used for estimating the exchange rate of non-reactive (conserved) species from their concentration gradient (e.g., Mayer et al., 2011 and references therein). Similarity theory holds for conserved tracers when observations of fluxes are made above the roughness sublayer (Raupach and Legg, 1984) and this criterion was met at BEARPEX 2009 (18 m flux measurement height with 8.8 m mean tree height), as evidenced by a comparison of the flux data of the sensible heat and 3 biogenic VOC species, methanol, 2-methyl-3-butene-2-ol +isoprene, and monoterpene, with longer chemical lifetimes than the turbulent transport time (Park et al., 2014).

The fluxes of reactive species cannot be completely described through simple application of similarity theory. This is because reactive species will, to some extent, undergo chemical transformations faster than they will be transported by turbulent diffusion (Vila-Guerau de Arellano et al., 1993; Gao et al., 1991; Jacob and Wofsy, 1990). However, similarity theory is still a powerful tool, as quantifying the flux due to turbulence transport allows for the estimation of the effects of other within-canopy chemical processes.

A visual representation of the idea proposed in this study is shown in Fig. 8. The red line shows the gradient expected if flux–gradient similarity holds, and the blue line shows the gradient if the concentration is chemically, or otherwise, perturbed. This concept is known as localized near field (LNF) theory (Vandenhurk and Mcnaughton, 1995; Raupach, 1989). We apply LNF to conserved tracers and reactive molecules to test (1) whether the flux–gradient theory is valid within the canopy at this site and (2) whether the chemical reactivity or some other canopy processes affects the reactive chemicals. In the analysis below, we will assess the within-canopy behavior of H_2O as conserved tracer and NO, NO_2, and NO_x through pictorial relationships analogous to Fig. 8.

In Fig. 8, the green dashed line divides two layers: a within-canopy layer and an above-canopy layer. C_{ABOVE} is the measured concentration in the above-canopy layer and C_{WITHIN} is the measured concentration within the canopy. Using similarity theory and the measured fluxes, we calculate $C_{\mathrm{CONSERVED}}$, the concentration that would be observed for a conserved tracer. The difference between C_{WITHIN} and $C_{\mathrm{CONSERVED}}$ defines C_{DELTA}, which represents the contribution to the concentration by non-conservative processes that act to perturb the flux gradient relationship. To quantify $C_{\mathrm{CONSERVED}}$ we use flux–gradient similarity, Eq. (2), (Meyer, 1986) and the mixing rate, K, the so-called eddy diffusivity constant, which is inferred from the observed sensible heat flux and temperature gradient.

$$\frac{\partial(C_{\mathrm{CONSERVED}} - C_{\mathrm{ABOVE}})}{\partial z} = \frac{\mathrm{Flux}}{K}. \quad (2)$$

In an illustrative test of our approach we present our results for the conserved tracer, water. In Fig. 9, the blue circles represent the measured gradient of H_2O and the red circles show the gradient inferred from the H_2O flux ($C_{\mathrm{CONSERVED}}$) in the within-canopy layer at midday (from 12:00 to 14:00). The difference between C_{WITHIN} and $C_{\mathrm{CONSERVED}}$ in the within-canopy layer, C_{DELTA}, shown as a black arrow, is small (1 % relative to C_{ABOVE} and within the concentration measurement uncertainty of 3 %; the estimated propagated error is 15 % based on 10 % error in sensible heat flux calculation and 10 % error in K estimation). The small difference of $C_{\mathrm{DELTA,H_2O}}$ is possibly due to the source/sink process difference with temperature and H_2O. However, the magnitude of C_{DELTA} is smaller than the estimated uncertainty, so we conclude that the sources/sink difference in H_2O and temperature are not detectable and the flux–gradient similarity holds for conserved tracer even within canopy at this site. This implies there is no measurable additional source/sink process(es) for H_2O, aside from turbulent transport, and the open canopy structure allows us to use flux–gradient similarity using within-canopy information. Similar results were obtained for CO_2 and several slowly reacting BVOCs (Park et al., 2014).

Applying the same analysis to NO and NO_2 (Fig. 10), we find C_{DELTA} is large compared to the measurement variability. C_{DELTA} for NO is -12.4 ± 3.3 ppt (23 % relative to C_{ABOVE}) and for NO_2 is 64.7 ± 4.7 ppt (44 % relative to C_{ABOVE}). We reach an identical conclusion, with slight numerical differences, if we reference the calculation to the canopy top height instead of the average through the canopy, finding 27 and 39 % differences for NO and NO_2 compared to the C_{ABOVE}, respectively. The estimated uncertainty in the C_{DELTA} calculation is 30 and 25 % (3.7 and 16.2 ppt) for NO and NO_2 based on the error propagation. The paired t test also shows statistically meaningful differences between C_{WITHIN} and $C_{\mathrm{CONSERVED}}$ for NO and NO_2 ($p < 0.01$). Examples of C_{DELTA} analysis from individual days are shown in Sect. S2 of the Supplement.

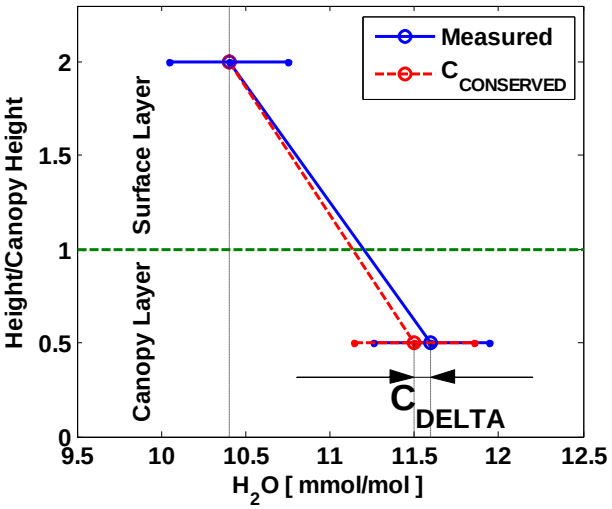

Figure 9. The estimated concentration, $C_{\mathrm{CONSERVED}}$ (red) using standard flux–gradient similarities of H_2O during midday (12:00–14:00) is shown. Blue represents the measured vertical gradient. Open circles and whiskers represent the mean and the variability of H_2O. The difference between blue and red in the within-canopy level is shown by the black arrow and indicates C_{DELTA} and is negligibly small, as expected for a conserved species.

Based on the observed gradient of NO, standard flux–gradient similarity predicts the downward flux of NO; however, we observed an upward flux of NO (Fig. 7). This counter-gradient flux can only be explained by the formation of NO during the transport process from within the canopy layer to the above-canopy layer. Fig. 10a indicates that to explain the observed NO flux, we need to account for 12 ppt (C_{DELTA}) more NO molecules than were observed in the canopy layer. This is reasonable, as photolysis rates above the canopy should be faster than in the shade of the canopy. If the required NO were completely due to NO_2 photolysis it would correspond to $\sim$12 ppt removal, or 20 % of the C_{DELTA} of NO_2. The remaining 80 % of C_{DELTA} in NO_2, 52.3 ppt, must be accounted for via other mechanisms.

To evaluate the contribution of photolysis of NO_2 to the counter-gradient flux of NO, we calculate the chemical conversion rate integrated over the 100 s (τ_{turb}) as Eq. (3).

$$P_{\mathrm{NO,net}} = L_{\mathrm{NO_2,net}} = j_{\mathrm{NO_2}}\mathrm{NO2} \quad (3)$$
$$-(k_{\mathrm{NO+O_3}}[\mathrm{O_3}] + k_{\mathrm{NO+HO_2}}[\mathrm{HO_2}] + k_{\mathrm{NO+RO_2}}[\mathrm{RO_2}])[\mathrm{NO}]$$

The photolysis rate, $j_{\mathrm{NO_2}}$, is calculated with the Tropospheric Ultraviolet and Visible (TUV) radiation model scaled to the measured PAR. We treat RO_2 as equal to HO_2. Using the measured concentrations of NO, NO_2, O_3, HO_2, and temperature, we estimate a net loss of 22.8 ppt (over 100 s) of NO_2, which is in excess of that needed to explain the NO counter-gradient flux of 12.4 ($\pm$3.3) ppt.

The large value of C_{DELTA} for NO_x (54.3 ± 5.9 ppt, 29 % relative to C_{ABOVE}) indicates the necessity of one or more

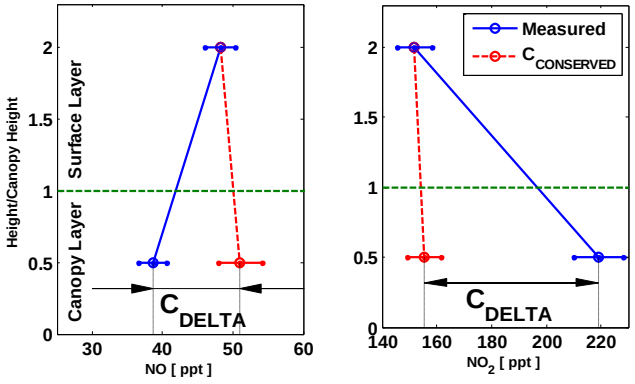

Figure 10. The estimated concentration, $C_{\mathrm{CONSERVED}}$, (red) using standard flux–gradient similarities of NO and NO_2 at midday (12:00–14:00 and the measured vertical gradient (blue), giving values for C_{DELTA} of 12 ppt (NO) and 64 ppt (NO_2).

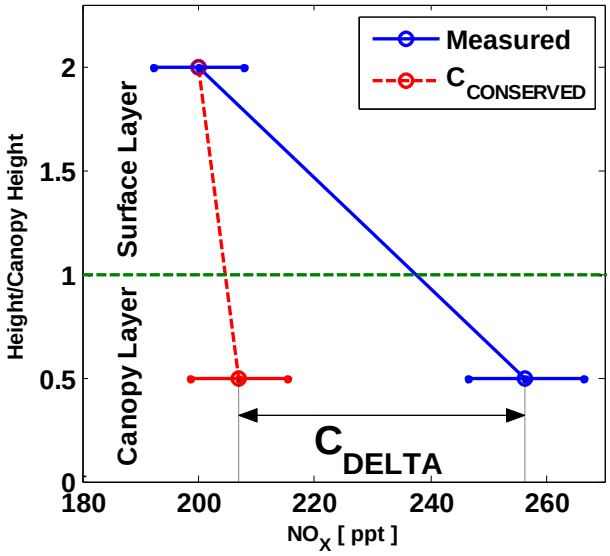

Figure 11. The estimated concentration, $C_{\mathrm{CONSERVED}}$, (red) using standard flux–gradient similarities of NO_x at midday (12:00–14:00) and the measured vertical gradient (blue) giving values for C_{DELTA} of 54 ppt (NO_x). Open circles and whiskers are the mean and standard errors.

within-canopy loss processes. To explore the mechanism(s) controlling the C_{DELTA} for NO_x, we examine several chemical processes related to PNs, ANs, HNO_3, and HONO using our two-layer model (concept shown in Fig. 8). The magnitudes of each of the near-field processes for NO_x were inferred using Eq. (4) to estimate the contribution of certain processes on the ~ 100 s timescale of turbulent mixing (τ_{turb}).

$$L_X \text{ or } P_X = \frac{\partial}{\partial t}\int_{z1}^{z2} C_X(z)\mathrm{d}z \tag{4}$$

Here, L_X (P_X) is the loss (production) rate of species X happening within the time window of turbulent air movement from within the canopy (height z_1) to above the canopy (height z_2). We chose 4.4 m, the middle level of the canopy, as a representative of z_1, and 18 m above-canopy layer as representative of z_2.

PNs can act as either a net source or a sink of NO_x through thermal dissociation ($+1$ NO_2 molecule) or PN formation (-1 NO_2). Calculating the steady-state chemical production and thermal and chemical loss of PAN (LaFranchi et al., 2009; Wolfe et al., 2009), yields 5.3 ppt of NO_2 formed in 100 s. This mechanism implies an enhancement of NO_x within the canopy, as discussed in more detail in Min et al. (2014). However, we have also suggested that a local biogenic precursor drives PN formation within canopy (Min et al., 2012). This BVOC PN species, denoted XPN, exhibited an upward flux and is a candidate for NO_2 loss not included in our steady-state calculation. We estimate the flux of this XPN to be 2.3 ± 0.4 ppt m s^{-1} corresponding to 16.7 ppt of NO_2 loss within canopy and explaining 31 % of the $NO_x C_{\mathrm{DELTA}}$.

BVOC-driven AN formation from OH initiated chemistry can be calculated as

$$P_{\sum \mathrm{AN}} = \sum_i \gamma_i \alpha_i k_{\mathrm{OH+VOC}_i}[\mathrm{OH}][\mathrm{VOC}_i], \tag{5}$$

where

$$\gamma_i = \frac{k_{\mathrm{RO_2}i+\mathrm{NO}}[\mathrm{NO}]}{k_{\mathrm{RO_2}i+\mathrm{NO}}[\mathrm{NO}] + k_{\mathrm{RO_2}i+\mathrm{HO_2}}[\mathrm{HO_2}] + \sum_j k_{\mathrm{RO_2}i+\mathrm{RO_2}j}[\mathrm{RO_2}]_j + k_{\mathrm{isom}}}. \tag{6}$$

Here, α_i and γ_i stands for the branching ratio of AN formation from RO_2 and NO reaction, and the fraction of RO_{2i} from VOC_i reacts with NO. Also, k_{isom} refers to the unimolecular isomerization rate of RO_{2i}. We estimate the effects of MBO, monoterpenes and isoprene (important BVOCs at the BEARPEX site (Bouvier-Brown et al., 2009a; Schade et al., 2000) on AN production (for 100 s) and calculate that 3.1 ppt (5.7 %), 0.4 ppt (0.7 %) and 6.9 ppt (12.8 %) NO_x is removed by AN formation, respectively. We use a 10, 11.7 and 18 % branching ratio (α_i) for MBO (Chan et al., 2009), isoprene (Paulot et al., 2009) and monoterpenes (Paulot et al., 2009). The rate constants and mechanisms for RO_2+HO_2, RO_2+NO and RO_2+RO_2 were taken from the Master Chemical Mechanism (MCM) v3.2 (Jenkin et al., 1997; Saunders et al., 2003) and isomerization rates for isoprene from Crounse et al. (2011). If we consider AN formation from ozonolysis reactions of very reactive BVOCs, such as sesquiterpenes in analogy to XPN formation through the channel described as BCSOZNO3 in MCM v3.2, we estimate an additional 16.8 ppt (31.1 %) of NO_x consumed over 100 s. These calculations indicate chemical formation of nitrates is rapid enough to affect the fluxes.

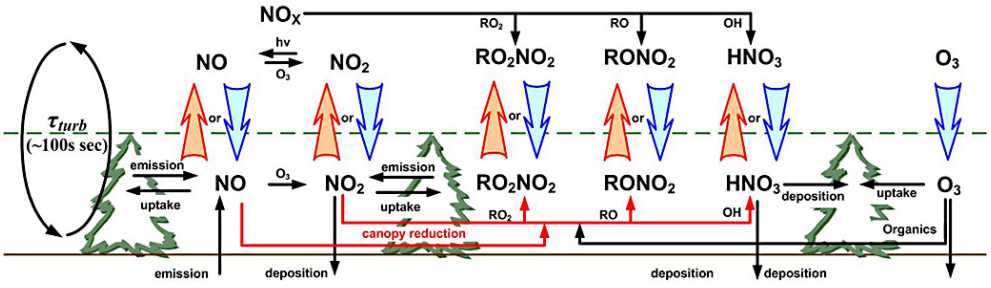

Figure 12. Schematic of the interactions involved in the exchange of nitrogen oxides between the atmosphere and the forest canopy as identified in this manuscript. Bold arrows in blue (downward) and red (upward) represent the direction of the flux of each species across the canopy surface. Red thin arrows within canopy indicate the NO_x removal processes within the canopy in addition to plant uptake.

Table 2. Possible within canopy NO_x consumption mechanisms.

Mechanisms	NO_x consumption [%]	[ppt]
Unidentified PN formation	30.8 %	16.7 ppt
MBO and monoterpene nitrates	19.2 %	10.4 ppt
Sesquiterpene nitrate	0–30.9 %	0–16.8 ppt
HNO_3	0.6–2.0 %	0.3–1.1 ppt
HONO*	< −1.8 %	< −1.0 ppt
Plant uptake	< 4.6 %	< 2.5 ppt
Total NO_x loss	53.4–85.7 %	28.9–46.5 ppt

Negative consumption indicates a source of NO_x within the canopy.

Formation of HNO_3 is also a potentially important pathway for the removal of NO_x from the system by wet and dry deposition after formation. The gas-phase reaction of NO_2 with OH is the major source of HNO_3 formation (heterogeneous formation HNO_3 from NO_2 hydrolysis is slower by an order of magnitude than the gas-phase formation rate), although hydrolysis of tertiary organic nitrates may also be important (Darer et al., 2011; Hu et al., 2011; Browne et al., 2013). The production rate can be calculated as

$$P_{HNO_3} = k_{OH+NO_2}[OH][NO_2]. \quad (7)$$

Using the measured OH concentration, we estimate 0.6–2 % of NO_x is lost through gas-phase reaction at this site. Compared to ANs and PNs, HNO_3 formation by OH reactions is unimportant.

HONO formation is another candidate for altering the flux of NO_x. HONO flux measurements at this site were observed to be small (-0.11 ± 0.69 ppt m s^{-1}) and slightly downward, contributing to the enhancement of NO_x within canopy rather than loss.

Direct uptake through plant stomata might be responsible for the remaining NO_2 removal within the canopy. We estimate < 2.5 ppt of NO_2 is removed through plant leaves at the typical daytime NO_2 concentration and canopy conductance (< 1 cm s^{-1} with 3.7 m^2 m^{-2}) assuming uptake rates similar to those reported in recent field and laboratory studies (Chapparro-Suarez et al., 2011; Breuninger et al., 2012; Breuninger et al., 2013). However, the daytime NO_2 concentration at this site of less than few hundred ppt suggests this site is a regime where NO_2 emissions from plant biota likely dominate, consistent with the results of Breuninger et al. (2013) who estimate 0.05–0.65 ppb as NO_2 compensation point in a Norway Spruce forest. Further evidence for an NO_2 compensation point from canopy-scale observations will be presented in Min et al. (2014).

Taken together, as much as 86 % of the C_{DELTA} for NO_x (Table 2) can be explained by local chemical NO_x loss mechanisms and the formation of higher nitrogen oxides. Given the uncertainties, it is reasonable to interpret this as indicative that all of the C_{DELTA} is due to within-canopy chemistry. This leads us to suggest a conceptual model for biosphere–atmosphere exchange of NO_x as shown in Fig. 12. In addition to the previously suggested within-canopy process of NO_x (Fig. 1), chemical pathways are added, converting NO_x to higher oxides of nitrogen. These pathways are alternative mechanisms to plant uptake that have the effect of reducing the soil NO that escapes the forest canopy. The direction and magnitude of higher nitrogen oxides fluxes in this coupled mechanism are then the net resultant of upward (owing to formation within canopy) and downward (deposition from the atmosphere) fluxes of each class.

6 Conclusions

During the BEARPEX 2009 field experiment, we observed upward fluxes of NO and NO_2 using eddy covariance flux measurements, along with large NO_2 and NO_x concentration enhancements within the canopy, and counter-gradient fluxes of NO. Applying standard flux–gradient relationships to interpret the data indicates the existence of one or more NO_x loss processes within the canopy, in addition to conversion of NO to NO_2 by reaction with O_3. We interpret these results as observational evidence for an ecosystem-scale chemical canopy reduction process and suggest these reactions may be a partial mechanistic explanation for the "canopy reduction factor" that has been relied on to reconcile

discordance between leaf-level, soil-level, and atmospheric modeling studies.

We investigate multiple chemical and ecophysiological processes to explain the NO_x removal during vertical transport and conclude that the chemical formation of PNs and ANs (and their vertical transport before they cycle back to NO_x) are the primary mechanisms responsible – implying that the reactive nitrogen does escape the canopy and may be returned as NO_x by further chemistry downwind.

The Supplement related to this article is available online at doi:10.5194/acp-14-5495-2014-supplement.

Acknowledgements. This research was supported by the National Science Foundation (grants NSF-AGS 1120076 and ATM-0639847). We thank S. Pacific Industries for use of their land, and the University of California, Berkeley, Blodgett Forest Research Station for cooperation in facilitating this research. We also thank D. D. Baldocchi for helpful comments on EC flux.

Edited by: I. Trebs

References

Anderson, I. C. and Poth, M. A.: Semiannual losses of nitrogen as NO and N_2O from unburned and burned chaparral, Global Biogeochem. Cy., 3, 121–135, 1989.

Baldocchi, D. D., Hicks, B. B., and Meyers, T. P.: Measuring Biosphere-Atmosphere Exchanges of Biologically Related Gases with Micrometeorological Methods, Ecology, 69, 1331–1340, 1988.

Bargsten, A., Falge, E., Pritsch, K., Huwe, B., and Meixner, F. X.: Laboratory measurements of nitric oxide release from forest soil with a thick organic layer under different understory types, Biogeosciences, 7, 1425–1441, doi:10.5194/bg-7-1425-2010, 2010.

Bouvier-Brown, N. C., Goldstein, A. H., Gilman, J. B., Kuster, W. C., and de Gouw, J. A.: In-situ ambient quantification of monoterpenes, sesquiterpenes, and related oxygenated compounds during BEARPEX 2007: implications for gas- and particle-phase chemistry, Atmos. Chem. Phys., 9, 5505–5518, doi:10.5194/acp-9-5505-2009, 2009a.

Bouvier-Brown, N. C., Holzinger, R., Palitzsch, K., and Goldstein, A. H.: Large emissions of sesquiterpenes and methyl chavicol quantified from branch enclosure measurements, Atmos. Environ., 43, 389–401, doi:10.1016/j.atmosenv.2008.08.039, 2009b.

Breuninger, C., Oswald, R., Kesselmeier, J., and Meixner, F. X.: The dynamic chamber method: trace gas exchange fluxes (NO, NO_2, O_3) between plants and the atmosphere in the laboratory and in the field, Atmos. Meas. Tech., 5, 955–989, doi:10.5194/amt-5-955-2012, 2012.

Breuninger, C., Meixner, F. X., and Kesselmeier, J.: Field investigations of nitrogen dioxide (NO_2) exchange between plants and the atmosphere, Atmos. Chem. Phys., 13, 773–790, doi:10.5194/acp-13-773-2013, 2013.

Browne, E. C., Min, K.-E., Wooldridge, P. J., Apel, E., Blake, D. R., Brune, W. H., Cantrell, C. A., Cubison, M. J., Diskin, G. S., Jimenez, J. L., Weinheimer, A. J., Wennberg, P. O., Wisthaler, A., and Cohen, R. C.: Observations of total $RONO_2$ over the boreal forest: NO_x sinks and HNO_3 sources, Atmos. Chem. Phys., 13, 4543–4562, doi:10.5194/acp-13-4543-2013, 2013.

Brummer, C., Marx, O., Kutsch, W., Ammann, C., Wolff, V., Flechard, C. R., and Freibauer, A.: Fluxes of total reactive atmospheric nitrogen (Sigma N-r) using eddy covariance above arable land, Tellus B, 65, 19770, doi:10.3402/tellusb.v65i0.19770, 2013.

Butterbach-Bahl, K., Breuer, L., Gasche, R., Willibald, G., and Papen, H.: Exchange of trace gases between soils and the atmosphere in Scots pine forest ecosystems of the northeastern German lowlands 1. Fluxes of N_2O, NO/NO_2 and CH_4 at forest sites with different N-deposition, Forest Ecol. Manag., 167, 123–134, 2002.

Chan, A. W. H., Galloway, M. M., Kwan, A. J., Chhabra, P. S., Keutsch, F. N., Wennberg, P. O., Flagan, R. C., and Seinfeld, J. H.: Photooxidation of 2-Methyl-3-Buten-2-ol (MBO) as a Potential Source of Secondary Organic Aerosol, Environ. Sci. Technol.,43, 4647–4652, doi:10.1021/es902789a, 2009.

Chaparro-Suarez, I. G., Meixner, F. X., and Kesselmeier, J.: Nitrogen dioxide (NO_2) uptake by vegetation controlled by atmospheric concentrations and plant stomatal aperture, Atmos. Environ., 45, 5742–5750, doi:10.1016/j.atmosenv.2011.07.021, 2011.

Chen, X. Y., Mulder, J., Wang, Y. H., Zhao, D. W., and Xiang, R. J.: Atmospheric deposition, mineralization and leaching of nitrogen in subtropical forested catchments, South China, Environ. Geochem. Hlth., 26, 179–186, 2004.

Choi, W., Faloona, I. C., McKay, M., Goldstein, A. H., and Baker, B.: Estimating the atmospheric boundary layer height over sloped, forested terrain from surface spectral analysis during BEARPEX, Atmos. Chem. Phys., 11, 6837–6853, doi:10.5194/acp-11-6837-2011, 2011.

Cleary, P. A., Wooldridge, P. J., and Cohen, R. C.: Laser-induced fluorescence detection of atmospheric NO_2 with a commercial diode laser and a supersonic expansion, Appl. Optics, 41, 6950–6956, 2002.

Crounse, J. D., Paulot, F., Kjaergaard, H. G., and Wennberg, P. O.: Peroxy radical isomerization in the oxidation of isoprene, Phys. Chem. Chem. Phys., 13, 13607, doi:10.1039/c1cp21330j, 2011.

Crutzen, P.: A discussion of the chemistry of some minor constituents in the stratosphere and troposphere, Pure Appl. Geophys., 106, 1385–1399, doi:10.1007/BF00881092, 1973

Darer, A. I., Cole-Filipiak, N. C., O'Connor, A. E., and Elrod, M. J.: Formation and Stability of Atmospherically Relevant Isoprene-Derived Organosulfates and Organonitrates, Environ. Sci. Technol., 45, 1895–1902, doi:10.1021/Es103797z, 2011.

Davidson, E. A., Matson, P. A., Vitousek, P. M., Riley, R., Dunkin, K., Garciamendez, G., and Maass, J. M.: Processes Regulating Soil Emissions of NO and N_2O in a Seasonally Dry Tropical Forest, Ecology, 74, 130–139, 1993.

Day, D. A., Wooldridge, P. J., Dillon, M. B., Thornton, J. A., and Cohen, R. C.: A thermal dissociation laser-induced fluorescence instrument for in situ detection of NO_2, peroxy nitrates, alkyl nitrates, and HNO_3, J. Geophys. Res., 107, 4045, doi:10.1029/2001jd000779, 2002.

Day, D. A., Dillon, M. B., Wooldridge, P. J., Thornton, J. A., Rosen, R. S., Wood, E. C., and Cohen, R. C.: On alkyl nitrates, O_3, and the "missing NO_y", J. Geophys. Res.-Atmos., 108, 4501, doi:10.1029/2003jd003685, 2003.

DiGangi, J. P., Boyle, E. S., Karl, T., Harley, P., Turnipseed, A., Kim, S., Cantrell, C., Maudlin III, R. L., Zheng, W., Flocke, F., Hall, S. R., Ullmann, K., Nakashima, Y., Paul, J. B., Wolfe, G. M., Desai, A. R., Kajii, Y., Guenther, A., and Keutsch, F. N.: First direct measurements of formaldehyde flux via eddy covariance: implications for missing in-canopy formaldehyde sources, Atmos. Chem. Phys., 11, 10565–10578, doi:10.5194/acp-11-10565-2011, 2011.

Dillon, M. B., Lamanna, M. S., Schade, G. W., Goldstein, A. H., and Cohen, R. C.: Chemical evolution of the Sacramento urban plume: Transport and oxidation, J. Geophys. Res.-Atmos., 107, 4045, doi:10.1029/2001jd000969, 2002.

Dorsey, J. R. , Duyzer, J. H., Gallagher, M. W., Coe, H., Pilegaard, K., Westrate, J. H., Jensen N. O., and Walton, S.: Oxidised Nitrogen and Ozone Interaction with Forests I: Experimental Observations and Analysis of Exchange with Douglas Fir, Q. J. Roy. Meteor. Soc., 130, 1941–1955, 2004.

Drummond, J. W., Volz, A., and Ehhalt, D. H.: An Optimized Chemi-Luminescence Detector for Tropospheric No Measurements, J. Atmos. Chem., 2, 287–306, 1985.

Duyzer, J. H., Dorsey, J. R., Gallagher, M. W., Pilegaard, K., and Walton, S.: Oxidised Nitrogen and Ozone Interaction with Forests II: A Multi-layer Model to Describe Above and Below Canopy Exchange and Processing, Q. J. Roy. Meteor. Soc., 130, 1957–1971, 2004.

Fares, S., McKay, M., Holzinger, R., and Goldstein, A. H.: Ozone fluxes in a Pinus ponderosa ecosystem are dominated by non-stomatal processes: Eveidence from long-term continuous measurements, Agric. Forest Meteorol., 150, 420–431, 2010.

Farmer, D. K., Wooldridge, P. J., and Cohen, R. C.: Application of thermal-dissociation laser induced fluorescence (TD-LIF) to measurement of HNO3, Σalkyl nitrates, Σperoxy nitrates, and NO_2 fluxes using eddy covariance, Atmos. Chem. Phys., 6, 3471–3486, doi:10.5194/acp-6-3471-2006, 2006.

Feig, G. T., Mamtimin, B., and Meixner, F. X.: Soil biogenic emissions of nitric oxide from a semi-arid savanna in South Africa, Biogeosciences, 5, 1723–1738, doi:10.5194/bg-5-1723-2008, 2008.

Foken, T.: Micrometeorology, Springer-Verlag, Berlin Heidelberg, Germany, 2006.

Foken, T. and Wichura, B.: Tools for quality assessment of surface-based flux measurements, Agr. Forest Meteorol., 78, 83–105, 1996.

Galloway, J. N., Dentener, F. J., Capone, D. G., Boyer, E. W., Howarth, R. W., Seitzinger, S. P., Asner, G. P., Cleveland, C. C., Green, P. A., Holland, E. A., Karl, D. M., Michaels, A. F., Porter, J. H., Townsend, A. R., and Vorosmarty, C. J.: Nitrogen cycles: past, present, and future, Biogeochemistry, 70, 153–226, 2004.

Gao, W., Wesely, M. L., and Lee, I. Y.: A Numerical Study of the Effects of Air Chemistry on Fluxes of NO, NO_2, and O_3 near the Surface, J. Geophys. Res.-Atmos., 96, 18761–18769, 1991.

Gasche, R. and Papen, H.: Spatial variability of NO and NO_2 flux rates from soil of spruce and beech forest ecosystems, Plant Soil, 240, 67–76, 2002.

Gbondo-Tugbawa, S. S. and Driscoll, C. T.: Evaluation of the effects of future controls on sulfur dioxide and nitrogen oxide emissions on the acid-base status of a northern forest ecosystem, Atmos. Environ., 36, 1631–1643, 2002.

Gut, A., Scheibe, M., Rottenberger, S., Rummel, U., Welling, M., Ammann, C., Kirkman, G. A., Kuhn, U., Meixner, F. X., Kesselmeier, J., Lehmann, B. E., Schmidt, W., Muller, E., and Piedade, M. T. F.: Exchange fluxes of NO_2 and O_3 at soil and leaf surfaces in an Amazonian rain forest, J. Geophys. Res.-Atmos., 107, 8060, doi:10.1029/2001jd000654, 2002a.

Gut, A., van Dijk, S. M., Scheibe, M., Rummel, U., Welling, M., Ammann, C., Meixner, F. X., Kirkman, G. A., Andreae, M. O., and Lehmann, B. E.: NO emission from an Amazonian rain forest soil: Continuous measurements of NO flux and soil concentration, J. Geophys. Res.-Atmos., 107, 8057, doi:10.1029/2001jd000521, 2002b.

Hereid, D. P. and Monson, R. K.: Nitrogen oxide fluxes between corn (Zea mays L.) leaves and the atmosphere, Atmos. Environ., 35, 975–983, 2001.

Herman, F., Smidt, S., Huber, S., Englisch, M., and Knoflacher, M.: Evaluation of pollution-related stress factors for forest ecosystems in central Europe, Environ Sci. Pollut. R., 8, 231–242, 2001.

Herman, D. J., Halverson, L. J., and Firestone, M. K.: Nitrogen dynamics in an annual grassland: oak canopy, climate, and microbial population effects, Ecol. Appl., 13, 593–604, 2003.

Hessen, D. O., Henriksen, A., Hindar, A., Mulder, J., Torseth, K., and Vagstad, N.: Human impacts on the nitrogen cycle: A global problem judged from a local perspective, Ambio, 26, 321–325, 1997.

Hietz, P., Turner, B. L., Wanek, W., Richter, A., Nock, C. A., and Wright, S. J.: Long-Term Change in the Nitrogen Cycle of Tropical Forests, Science, 334, 664–666, doi:10.1126/science.1211979, 2011.

Holland, E. A. and Lamarque, J. F.: Modeling bio-atmospheric coupling of the nitrogen cycle through NO_X emissions and NO_y deposition, Nutr. Cycl. Agroecosys., 48, 7–24, 1997.

Holland, E. A., Braswell, B. H., Lamarque, J. F., Townsend, A., Sulzman, J., Muller, J. F., Dentener, F., Brasseur, G., Levy, H., Penner, J. E., and Roelofs, G. J.: Variations in the predicted spatial distribution of atmospheric nitrogen deposition and their impact on carbon uptake by terrestrial ecosystems, J. Geophys. Res.-Atmos., 102, 15849–15866, 1997.

Holzinger, R., Lee, A., Paw, K. T., and Goldstein, U. A. H.: Observations of oxidation products above a forest imply biogenic emissions of very reactive compounds, Atmos. Chem. Phys., 5, 67–75, doi:10.5194/acp-5-67-2005, 2005.

Horii, C. V.: Tropospheric reactive nitrogen speciation, deposition and chemistry at Harvard Forest, Ph.D., Harvard University, Cambridge, MA, USA, 2002.

Horii, C. V., Munger, J. W., Wofsy, S. C., Zahniser, M., Nelson, D., and McManus, J. B.: Fluxes of nitrogen oxides over a temperate deciduous forest, J. Geophys. Res.-Atmos., 109, D08305, doi:10.1029/2003jd004326, 2004.

Hu, K. S., Darer, A. I., and Elrod, M. J.: Thermodynamics and kinetics of the hydrolysis of atmospherically relevant organonitrates and organosulfates, Atmos. Chem. Phys., 11, 8307–8320, doi:10.5194/acp-11-8307-2011, 2011.

Hungate, B. A., Dukes, J. S., Shaw, M. R., Luo, Y. Q., and Field, C. B.: Nitrogen and climate change, Science, 302, 1512–1513, 2003.

Jacob, D. J. and Wofsy, S. C.: Budgets of Reactive Nitrogen, Hydrocarbons, and Ozone over the Amazon-Forest during the Wet Season, J. Geophys. Res.-Atmos., 95, 16737–16754, 1990.

Jenkin, M. E., Saunders, S. M., and Pilling, M. J.: The tropospheric degradation of volatile organic compounds: a protocol for mechanism development, Atmos. Environ., 31, 81–104, doi:10.1016/S1352-2310(96)00105-7, 1997.

Kaimal, J. C. and Finnigan, J. J.: Atmospheric boundary layer flows: their structure and measurement, Oxford University Press, New York, NY, USA, 1994.

Karl, T., Harley, P., Guenther, A., Rasmussen, R., Baker, B., Jardine, K., and Nemitz, E.: The bi-directional exchange of oxygenated VOCs between a loblolly pine (*Pinus taeda*) plantation and the atmosphere, Atmos. Chem. Phys., 5, 3015–3031, doi:10.5194/acp-5-3015-2005, 2005.

Kurpius, M. R. and Goldstein, A. H.: Gas-phase chemistry dominates O_3 loss to a forest, implying a source of aerosols and hydroxyl radicals to the atmosphere, Geophys. Res. Lett., 30, 1371, doi:10.1029/2002gl016785, 2003.

LaFranchi, B. W., Wolfe, G. M., Thornton, J. A., Harrold, S. A., Browne, E. C., Min, K. E., Wooldridge, P. J., Gilman, J. B., Kuster, W. C., Goldan, P. D., de Gouw, J. A., McKay, M., Goldstein, A. H., Ren, X., Mao, J., and Cohen, R. C.: Closing the peroxy acetyl nitrate budget: observations of acyl peroxy nitrates (PAN, PPN, and MPAN) during BEARPEX 2007, Atmos. Chem. Phys., 9, 7623–7641, doi:10.5194/acp-9-7623-2009, 2009.

LaFranchi, B. W., Goldstein, A. H., and Cohen, R. C.: Observations of the temperature dependent response of ozone to NO_x reductions in the Sacramento, CA urban plume, Atmos. Chem. Phys., 11, 6945–6960, doi:10.5194/acp-11-6945-2011, 2011.

Lee, X., Massman, W., and Law, B.: Handbook of micrometeorology: a guide for surface flux measurement and analysis, Kluwer Academic Publishers, Dordrecht, the Netherlands, 2004.

Lerdau, M. T., Munger, L. J., and Jacob, D. J.: Atmospheric chemistry – The NO_2 flux conundrum, Science, 289, 2291–2293, doi:10.1126/science.289.5488.2291, 2000.

Li, D. J. and Wang, X. M.: Nitric Oxide Emission Following Wetting of Dry Soils in Subtropical Humid Forests, Pedosphere, 19, 692–699, doi:10.1016/S1002-0160(09)60164-8, 2009.

Lockwood, A. L., Filley, T. R., Rhodes, D., and Shepson, P. B.: Foliar uptake of atmospheric organic nitrates, Geophys. Res. Lett., 35, L15809, doi:10.1029/2008gl034714, 2008.

Makarov, M. I. and Kiseleva, V. V.: Acidification and nutrient imbalance in forest soils subjected to nitrogen deposition, Water Air Soil Poll., 85, 1137–1142, 1995.

Massman, W. J.: The Attenuation of Concentration Fluctuations in Turbulent-Flow through a Tube, J. Geophys. Res.-Atmos., 96, 15269–15273, 1991.

Mayer, J. C., Bargsten, A., Rummel, U., Meixner, F. X., and Foken, T.: Distributed Modified Bowen Ratio method for surface layer fluxes of reactive and non-reactive trace gases, Agr. Forest Meteorol., 151, 655–668, doi:10.1016/j.agrformet.2010.10.001, 2011.

McMillen, R. T.: An Eddy-Correlation Technique with Extended Applicability to Non-Simple Terrain, Bound.-Lay. Meteorol., 43, 231–245, 1988.

Meyer, K.: Effects of Fuel-Element Vibrations on Spectral Density of Neutron-Flux Fluctuations in Pressurized Water-Reactors, Kernenergie, 29, 49–50, 1986.

Min, K.-E., Pusede, S. E., Browne, E. C., LaFranchi, B. W., Wooldridge, P. J., Wolfe, G. M., Harrold, S. A., Thornton, J. A., and Cohen, R. C.: Observations of atmosphere-biosphere exchange of total and speciated peroxynitrates: nitrogen fluxes and biogenic sources of peroxynitrates, Atmos. Chem. Phys., 12, 9763–9773, doi:10.5194/acp-12-9763-2012, 2012.

Min, K.-E., Pusede, S. E., Browne, E. C., LaFranchi, B. W., Wooldridge, P. J., and Cohen, R. C.: Observational evidence for an ecosystem scale NO_2 compensation point, Atmos. Chem. Phys., in press, 2014.

Misson, L., Tang, J., Ming, X., McKay, M., and Goldstein, A. H.: Influences of recovery from clear-cut, climate variability, and thinning on the carbon balance of a young ponderosa pine plantation, Agric. Forest Meteorol., 130, 207–222, 2005.

Moore, C. J.: Frequency-Response Corrections for Eddy-Correlation Systems, Bound.-Lay. Meteorol., 37, 17–35, 1986.

Morikawa, H., Takahashi, M., Sakamoto, A., Matsubara, T., Arimura, G. I., Kawamura, Y., Fukunaga, K., Fujita, K., Sakurai, N., Hirata, T., Ide, H., Nonoyama, N., and Suzuki, H.: Formation of unidentified nitrogen in plants: an implication for a novel nitrogen metabolism, Planta, 219, 14–22, doi:10.1007/s00425-003-1200-7, 2004.

Morikawa, T., Oikawa, A., Wadano, A., Yano, K., Sakurai, N., Suzuki, H., Saito, K., Shibata, D., and Ohta, D.: Plant metabolomic analyses by FT-ICR/MS, GC/MS, and LC/MS, Plant Cell Physiol., 45, S206–S206, 2004.

Murphy, J. G., Day, D. A., Cleary, P. A., Wooldridge, P. J., Millet, D. B., Goldstein, A. H., and Cohen, R. C.: The weekend effect within and downwind of Sacramento – Part 1: Observations of ozone, nitrogen oxides, and VOC reactivity, Atmos. Chem. Phys., 7, 5327–5339, doi:10.5194/acp-7-5327-2007, 2007.

Neirynck, J., Kowalski, A. S., Carrara, A., Genouw, G., Berghmans, P., and Ceulemans, R.: Fluxes of oxidised and reduced nitrogen above a mixed coniferous forest exposed to various nitrogen emission sources, Environ. Pollut., 149, 31–43, 2007.

Norby, R. J., Warren, J. M., Iversen, C. M., Medlyn, B. E., and McMurtrie, R. E.: CO_2 enhancement of forest productivity constrained by limited nitrogen availability, P. Natl. Acad. Sci. USA, 107, 19368–19373, doi:10.1073/pnas.1006463107, 2010.

Oka, E., Tagami, Y., Oohashi, T., and Kondo, N.: A physiological and morphological study on the injury cause by exposure to the air pollutant, peroxyacetyl nitrate (PAN), based on the quantitative assessment of the injusry, J. Plant. Res., 117, 27–36, doi:10.1007/s10265-003-0127-1, 2004.

Ollinger, S. V., Aber, J. D., Reich, P. B., and Freuder, R. J.: Interactive effects of nitrogen deposition, tropospheric ozone, elevated CO_2 and land use history on the carbon dynamics of northern hardwood forests, Glob. Change Biol., 8, 545–562, 2002a.

Ollinger, S. V., Smith, M. L., Martin, M. E., Hallett, R. A., Goodale, C. L., and Aber, J. D.: Regional variation in foliar chemistry and N cycling among forests of diverse history and composition, Ecology, 83, 339–355, 2002b.

Ordin, L., Garber, M. J., Kindinge, J., Whitmore, S. A., Greve, L. C., and Taylor, O. C.: Effect of Peroxyacetyl Nitrate (PAN) in-Vivo

on Tobacco Leaf Polysaccharide Synthetic Pathways Enzymes, Environ. Sci. Technol., 5, 621–626, 1971.

Park, J.-H., Goldstein, A. H., Timkovsky, J., Fares, S., Weber, R., Karlik, J., and Holzinger, R.: Active atmosphere-ecosystem exchange of the vast majority of detected volatile organic compounds, Science, 341, 643–647, doi:10.1126/science.1235053, 2013.

Park, J.-H., Fares, S., Weber, R., and Goldstein, A. H.: Biogenic volatile organic compound emissions during BEARPEX 2009 measured by eddy covariance and flux-gradient similarity methods, Atmos. Chem. Phys., 14, 231–244, doi:10.5194/acp-14-231-2014, 2014.

Paulot, F., Crounse, J. D., Kjaergaard, H. G., Kroll, J. H., Seinfeld, J. H., and Wennberg, P. O.: Isoprene photooxidation: new insights into the production of acids and organic nitrates, Atmos. Chem. Phys., 9, 1479–1501, doi:10.5194/acp-9-1479-2009, 2009.

Pawlowski, L.: Acidification: its impact on the environment and mitigation strategies, Ecol. Eng., 8, 271–288, 1997.

Raivonen, M., Keronen, P., Vesala, T., Kulmala, M., and Hari, P.: Measuring shoot-level NO_X flux in field conditions: the role of blank chambers, Boreal Environ. Res., 8, 445–455, 2003.

Raivonen, M., Vesala, T., Pirjola, L., Altimir, N., Keronen, P., Kulmala, M., and Hari, P.: Compensation point of NO_X exchange: Net result of NO_X consumption and production, Agr. Forest Meteorol., 149, 1073–1081, doi:10.1016/j.agrformet.2009.01.003, 2009.

Raupach, M. R. and Legg, B. J.: The Uses and Limitations of Flux-Gradient Relationships in Micrometeorology, Agr. Water Manage., 8, 119–131, 1984.

Raupach, M. R.: A Practical Lagrangian Method for Relating Scalar Concentrations to Source Distributions in Vegetation Canopies, Q. J. Roy. Meteor. Soc., 115, 609–632, 1989.

Ren, X., Sanders, J. E., Rajendran, A., Weber, R. J., Goldstein, A. H., Pusede, S. E., Browne, E. C., Min, K.-E., and Cohen, R. C.: A relaxed eddy accumulation system for measuring vertical fluxes of nitrous acid, Atmos. Meas. Tech., 4, 2093–2103, doi:10.5194/amt-4-2093-2011, 2011.

Rummel, U., Ammann, C., Gut, A., Meixner, F. X., and Andreae, M. O.: Eddy covariance measurements of nitric oxide flux within an Amazonian rain forest, J. Geophys. Res.-Atmos., 107, 8050, doi:10.1029/2001jd000520, 2002.

Russell, A. R., Valin, L. C., Bucsela, E. J., Wenig, M. O., and Cohen, R. C.: Space-based Constraints on Spatial and Temporal Patterns of NO_X Emissions in California, 2005–2008, Environ. Sci. Technol., 44, 3608–3615, doi:10.1021/Es903451j, 2010.

Ruuskanen, T. M., Müller, M., Schnitzhofer, R., Karl, T., Graus, M., Bamberger, I., Hörtnagl, L., Brilli, F., Wohlfahrt, G., and Hansel, A.: Eddy covariance VOC emission and deposition fluxes above grassland using PTR-TOF, Atmos. Chem. Phys., 11, 611–625, doi:10.5194/acp-11-611-2011, 2011.

Saunders, S. M., Jenkin, M. E., Derwent, R. G., and Pilling, M. J.: Protocol for the development of the Master Chemical Mechanism, MCM v3 (Part A): tropospheric degradation of non-aromatic volatile organic compounds, Atmos. Chem. Phys., 3, 161–180, doi:10.5194/acp-3-161-2003, 2003.

Schade, G. W., Goldstein, A. H., Gray, D. W., and Lerdau, M. T.: Canopy and leaf level 2-methyl-3-buten-2-ol fluxes from a ponderosa pine plantation, Atmos. Environ., 34, 3535–3544, 2000.

Seok, B., Helmig, D., Ganzeveld, L., Williams, M. W., and Vogel, C. S.: Dynamics of nitrogen oxides and ozone above and within a mixed hardwood forest in northern Michigan, Atmos. Chem. Phys., 13, 7301–7320, doi:10.5194/acp-13-7301-2013, 2013.

Sparks, J. P.: Ecological ramifications of the direct foliar uptake of nitrogen, Oecologia, 159, 1–13, doi:10.1007/s00442-008-1188-6, 2009.

Sparks, J. P., Monson, R. K., Sparks, K. L., and Lerdau, M.: Leaf uptake of nitrogen dioxide (NO_2) in a tropical wet forest: implications for tropospheric chemistry, Oecologia, 127, 214–221, 2001.

Takahashi, M., Nakagawa, M., Konaka, D., Sakamoto, A., Matsubara, T., Ohsumi, C., Suzuki, H., and Morikawa, H.: Urban NO_X "pollution" is a plant vitalization signal, Plant Cell Physiol., 45, S125–S125, 2004.

Takahashi, M., Nakagawa, M., Sakamoto, A., Ohsumi, C., Matsubara, T., and Morikawa, H.: Atmospheric nitrogen dioxide gas is a plant vitalization signal to increase plant size and the contents of cell constituents, New Phytol., 168, 149–153, doi:10.1111/j.1469-8137.2005.01493.x, 2005a.

Takahashi, M., Nakayama, N., and Arihara, J.: Plant nitrogen levels and photosynthesis in the supernodulating soybean (Glycine max L. Merr.) cultivar 'Sakukei 4', Plant Prod. Sci., 8, 412–418, 2005b.

Teklemariam, T. A. and Sparks, J. P.: Gaseous fluxes of peroxyacetyl nitrate (PAN) into plant leaves, Plant Cell Environ., 27, 1149–1158, 2004.

Thornton, J. A., Wooldridge, P. J., and Cohen, R. C.: Atmospheric NO_2: In situ laser-induced fluorescence detection at parts per trillion mixing ratios, Anal. Chem., 72, 528–539, 2000.

Townsend, A. R., Braswell, B. H., Holland, E. A., and Penner, J. E.: Spatial and temporal patterns in terrestrial carbon storage due to deposition of fossil fuel nitrogen, Ecol. Appl., 6, 806–814, 1996.

Turnipseed, A. A., Huey, L. G., Nemitz, E., Stickel, R., Higgs, J., Tanner, D. J., Slusher, D. L., Sparks, J. P., Flocke, F., and Guenther, A.: Eddy covariance fluxes of peroxyacetyl nitrates (PANs) and NO(y) to a coniferous forest, J. Geophys. Res.-Atmos., 111, D09304, doi:10.1029/2005jd006631, 2006.

Vandenhurk, B. J. J. M. and Mcnaughton, K. G.: Implementation of near-Field Dispersion in a Simple 2-Layer Surface-Resistance Model, J. Hydrol., 166, 293–311, 1995.

van Dijk, S. M., Gut, A., Kirkman, G. A., Meixner, F. X., Andreae, M. O., and Gomes, B. M.: Biogenic NO emissions from forest and pasture soils: Relating laboratory studies to field measurements, J. Geophys. Res.-Atmos., 107, 8058, doi:10.1029/2001jd000358, 2002.

Vila-Guerau de Arellano, J., Duynkerke, P. G., and Builtjes, P. J. H.: The Divergence of the Turbulent-Diffusion Flux in the Surface-Layer Due to Chemical-Reactions – the NO-O_3-NO_2 System, Tellus B, 45, 23–33, 1993.

Vitousek, P. M. and Farrington, H.: Nutrient limitation and soil development: Experimental test of a biogeochemical theory, Biogeochemistry, 37, 63–75, 1997.

Vitousek, P. M., Aber, J. D., Howarth, R. W., Likens, G. E., Matson, P. A., Schindler, D. W., Schlesinger, W. H., and Tilman, D. G.: Human alteration of the global nitrogen cycles: sources and consequences, Ecol. Appl., 7, 737–750, 1997.

Wang, Y. P. and Leuning, R.: A two-leaf model for canopy conductance, photosynthesis and partitioning of available energy I:

Model description and comparison with a multi-layered model, Agr. Forest Meteorol., 91, 89–111, 1998.

Wesely, M. L., Eastman, J. A., Stedman, D. H., and Yalvac, E. D.: An eddy-correlation measurement of NO_2 flux to vegetation and comparison to O_3 flux, Atmos. Environ., 16, 815–820, 1982.

Wildt, J., Kley, D., Rockel, A., Rockel, P., and Segschneider, H. J.: Emission of NO from several higher plant species, J. Geophys. Res.-Atmos., 102, 5919–5927, 1997.

Wolfe, G. M., Thornton, J. A., Yatavelli, R. L. N., McKay, M., Goldstein, A. H., LaFranchi, B., Min, K.-E., and Cohen, R. C.: Eddy covariance fluxes of acyl peroxy nitrates (PAN, PPN and MPAN) above a Ponderosa pine forest, Atmos. Chem. Phys., 9, 615–634, doi:10.5194/acp-9-615-2009, 2009.

Wolfe, G. M., Thornton, J. A., Bouvier-Brown, N. C., Goldstein, A. H., Park, J.-H., McKay, M., Matross, D. M., Mao, J., Brune, W. H., LaFranchi, B. W., Browne, E. C., Min, K.-E., Wooldridge, P. J., Cohen, R. C., Crounse, J. D., Faloona, I. C., Gilman, J. B., Kuster, W. C., de Gouw, J. A., Huisman, A., and Keutsch, F. N.: The Chemistry of Atmosphere-Forest Exchange (CAFE) Model – Part 2: Application to BEARPEX-2007 observations, Atmos. Chem. Phys., 11, 1269–1294, doi:10.5194/acp-11-1269-2011, 2011.

Yienger, J. J. and Levy, H.: Empirical-Model of Global Soil-Biogenic NO_X Emissions, J. Geophys. Res.-Atmos., 100, 11447–11464, 1995.

Yu, J. B., Meixner, F. X., Sun, W. D., Mamtimin, B., Xia, C. H., and Xie, W. J.: Biogenic Nitric Oxide Emission of Mountain Soils Sampled from Different Vertical Landscape Zones in the Changbai Mountains, Northeastern China, Environ. Sci. Technol., 44, 4122–4128, doi:10.1021/Es100380m, 2010.

Zapletal, M., Chroust, P., and Kunak, D.: The relationship between defoliation of Norway spruce and atmospheric deposition of sulphur and nitrogen compounds in the Hruby Jesenik Mts (the Czech Republic), Ekol Bratislava, 22, 337–347, 2003.